A novel method for producing functionalized vesicles that efficiently deliver oligonucleotides *in vitro* and *in vivo in mice*[1,2]

Pragati Jain[3,4] and Arthur G. Roberts[3,4]

1. No part of this publication may be reproduced, stored in a retrieval system, or transmitted in any form or by any means, electronic, mechanical, photocopying, recording, or otherwise without prior written permission from both Pragati Jain and Dr. Arthur G. Roberts.
2. All the work was funded by an NIH R01 grant by the National Cancer Institute Grant (1R01CA204846-01A1).
3. Department of Pharmaceutical and Biomedical Sciences, University of Georgia, 30602.
4. Co-contributing authors: Ms. Pragati Jain (pragati.jain94@uga.edu); Dr. Arthur G. Roberts (audie@uga.edu).

Abstract

Nano-based delivery systems have greatly enhanced our ability to administer and target drugs and macromolecules to their therapeutic targets. Because of chemically modifying them and their functional effects on cells, oligonucleotide drugs have great therapeutic potential. Oligonucleotide drugs have off-target effects and stability issues, so they can be encapsulated functionalized vesicles with targeting ligands such as antibodies (Ab). Herein, we describe a novel, scalable and straightforward approach to produce functionalized vesicles, which we call the “Functionalized Lipid Insertion Method.” This method differs significantly from an older approach for producing functionalized vesicles referred to as the “Detergent-Dialysis Method.” The older method requires excess detergent and extensive dialysis over many hours to produce the functionalized vesicles. With the “Functionalized Lipid Insertion Method,” only the functionalized lipid is detergent-solubilized during the formation of the functionalized vesicle. The approach reduces the dialysis time, keeps the vesicle intact, and orients the functionalized lipid to improve targeting compared to the older method. The dynamic light scattering (DLS) technique demonstrates that vesicle size is sensitive to the initial solubilized component mixture by the older method. In contrast, functionalized vesicle size increases in size are consistent with functionalized lipid insertion into the vesicle. *In vitro*, functionalized vesicles using our approach are able to deliver oligonucleotides selectively and can functionally affect liver cancer HepG2 cells. Functionalized vesicles produced by this method can also achieve targeted delivery of oligonucleotides in mice without inducing a significant immune response through cytokine production or showing physical signs of an

immune response. The industrial and therapeutic significance and implications of functionalized vesicles produced by our method are also discussed.

Keywords: Drug delivery, oligonucleotides, liposomes, extracellular vesicles, bioengineering

Abbreviations: Ab, antibody; C_t, cycle threshold; CMC, critical micelle concentration; EMEM, Eagle's minimal essential medium (EMEM); EV, extracellular vesicle; FA, fatty acid; FBS, Fetal Bovine Serum; HepG2, human liver cancer cell line; HCC, hepatocellular carcinoma; LNP, liposomal nanoparticle; miR, microRNA; miRNA, microRNA; mEV, modified extracellular vesicle; mLNP, modified liposomal nanoparticle; PBS, phosphate-buffered saline.

Introduction

Nano-based delivery systems have been developed to deliver a wide range of molecules, including drugs, nucleotides, and proteins [1]. Several nano-based delivery systems are available, including liposomes, dendrimers, and carbon nanotubes [2]. To be effective *in vivo* carriers, they are designed to be biodegradable, biocompatible, and non-immunogenic [3–5]. Ideal nano-based delivery systems must overcome many challenges, including rapid clearance, instability, toxicity, and inefficient targeting [5–7].

Two major nano-based delivery systems recently employed are extracellular vesicles (EVs) and liposomal nanoparticles (LNPs) [e.g., 8,9]. EVs are naturally occurring vesicles with an average size generally around 200 nm in diameter excreted from various body fluids such as blood and urine [10]. Depending on their source, they can still range widely from ~20 nm to 10 μm in diameter [10]. In contrast, LNPs are artificially produced delivery systems and can be made in various sizes through different techniques [e.g., 9,11]. EVs are formed by inward budding of the plasma membrane with other surface membrane invaginations from the Golgi apparatus [11]. These play an essential role in cell-to-cell communication and naturally carry RNA and proteins as their internal cargo [11]. EVs are advantageous for drug delivery because of their inherent biocompatibility, long-circulating half-life, low toxicity, and tendency to be endocytosed into target tissues [12]. On the other hand, LNPs have a lot of therapeutic potential as they can be designed with improved biocompatibility, stored lyophilized for long periods, and produced on an industrial scale [13,14].

Artificial and natural functionalized vesicles have been engineered using relatively simple methods [15,16]. EVs have been covered with antibodies against the surface CD9

protein and had improved delivery of miRNA to effector T-cells [15] but seem limited to transfer between T-cells. Since the 1980s, an approach called the “Detergent-Dialysis Method” has been employed that uses detergent and dialysis to produce functionalized vesicles [17–24]. One of the key differences of this approach is that they completely detergent solubilize all the components and require extensive dialysis for detergent removal [17–24]. In addition, this approach disrupts the original structure of the vesicle by detergent solubilization [17–24]. The procedure is also very time-consuming because functionalized vesicle formation from detergent-solubilized components requires extensive dialysis [17–24]. A two-stage process for producing mEVs was developed recently where the EVs are PEGylated and attached with antibodies [16]. The three-day process has a lot of potential for industrial scale-up [16,25,26]. Unfortunately, the mEVs undergo large temperature fluctuations between 4°C and 40°C during manufacture that may destabilize constitutive proteins and antibodies (Abs) [16,25,26].

Oligonucleotide drugs can be natural or synthetic [27,28]. They have shown a lot of potential for treating diseases, and ten have been approved by the FDA [28]. Oligonucleotide drugs can be easily modified and produced, which is a major advantage over traditional small molecule drugs [29]. Most oligonucleotide drugs have sequences that complement their DNA or RNA targets [28]. Oligonucleotide drugs include small interfering RNAs (siRNA) [30,31], antisense oligonucleotides (ASOs) [32,33] and microRNAs (miRNAs) [34]. Some of the challenges of oligonucleotide drugs are inducing an immunogenic response, enzymatic degradation, and off-target effects [27].

SiRNA is generally recognized as a short 21-23 base pair double-stranded RNA (dsRNA) molecule with 2 x 3’ nucleotide overhangs [30]. They play a vital role in RNA

interference (RNAi), which is involved in cellular growth and differentiation [35]. They can also target several disease-causing genes, so several siRNAs are currently in different stages of drug development [30,36]. Unfortunately, siRNAs are also susceptible to enzymatic degradation, off-target gene silencing, and potential activation of the immune response [31]. Therefore, these nucleotide polymers have been chemically modified and delivered through nanoparticle delivery vehicles such as liposomes [31].

ASOs are short 15-25 base pair polynucleotides that can be designed to bind to disease-related targets [32,33]. Mechanistically, they bind to a target RNA, which induces RNA degradation [33]. They also cause steric hindrance by chemically modified ASOs inhibiting RNA degradation [33]. However, ASOs suffer from similar challenges as other oligonucleotide drugs, so they have been delivered by various means, including liposomes, cationic amphiphiles, and dendrimers [33,37].

Finally, a small polynucleotide called microRNA (miRNA) represents another potential therapeutic that can be delivered with functionalized vesicles by our approach [34]. These macromolecules are small non-coding polynucleotides that range in length between 17 and 25 nucleotides [38]. They play an essential role in physiology by modulating gene expression through binding to mRNA [38]. MiRNAs have been associated with many diseases, including several cardiovascular diseases, several types of cancer, and allergic responses [39]. They can also elicit anticancer drug resistance in cancerous tumors [40]. MiRNAs have served as biomarkers for various diseases, and their ability to modulate gene expression has a lot of therapeutic potential [34,39]. These miRNA therapeutics can be synthetic mimics or inhibitors called anti-miRs [34]. They have been chemically modified to reduce degradation and improve their therapeutic efficacy

[34]. These macromolecules have also been delivered by liposomes, dendrimers, and polymers [34]. Currently, several miRNA therapeutics are going through clinical trials to treat cancer and liver disease [34]. Therefore, targeted delivery of miRNA represents an excellent opportunity to test our approach to produce functionalized vesicles.

In this work, a more straightforward, less time-consuming, and non-disruptive approach for producing functionalized vesicles called the "Functionalized Lipid Insert Method" is described and differentiated from the older "Dialysis-Detergent Method" [17–24]. The functionalized vesicles can be produced much more efficiently than [16] and the older method [17–24]. Our new approach keeps the temperature constant (4°C) where vesicles, proteins, and Abs are stable [25,26,41]. The process has a relatively high surface Ab concentration that is 700-fold higher than the previous approach to modify EVs [16]. Functionalized vesicles can be produced with any targeting ligand or protein, such as antibodies and affibodies. These vesicles will give them the potential ability to target any cell, tissue, or organ. The *in vitro* targeting and functional effects of mEVs and mLNPs by our procedure are demonstrated with hepatocellular carcinoma (HCC) HepG2 cells. In mice, mEVs and mLNPs were designed with different Abs to target specific organs. The organ specificity of the mEVs and mLNPs seemed dependent on the targeting Ab. The potential commercial advantages of targeted therapeutic delivery using our approach are discussed.

Materials and Methods

Cell culture

Human donors were enrolled for blood collection in compliance with the World Medical Association's Declaration of Helsinki and the Human Research Protection Program and Institutional Review Board guidelines for human subject research at the University of Georgia. Enrolled healthy volunteers signed consent forms to inform them about the study. The human blood protocol (University of Georgia Institutional Review Board (IRB) no STUDY00006632) and the consent form were reviewed and approved by the IRB of the University of Georgia.

The human liver cancer HepG2 cells were purchased from American type culture collection (ATCC, Maryland, MD). These were grown and maintained in Eagle's minimum essential medium (EMEM) (Corning), which was supplemented with 10% fetal bovine serum (FBS) (Atlanta Biologicals, Flowery Branch, GA) and 5% penicillin/streptomycin (Thermo Fisher, Waltham, MA). These cells were incubated in a humidified atmosphere of 5% CO_2 at 37ºC.

Materials and Reagents

The conjugating fatty acid (FA) label, 1,2-distearoyl-sn-glycero-3-phosphoethanolamine-N-[maleimide(polyethylene glycol)-2000] (DSPE-PEG2000-maleimide), and fluorescent 1,2-distearoyl-sn-glycero-3-phosphoethanolamine-N-(7-nitro-2-1,3-benzoxadiazol-4-yl) (NBD-DSPE) were purchased from Avanti Polar lipids (Alabaster, AL). HEPES (4-(2-hydroxyethyl)-1-piperazineethanesulfonic acid), n-dodecyl-β-D-maltoside (DDM) detergent, and Histopaque 1077 Reagent were purchased from Sigma Aldrich (St. Louis, MO). For the construction of liposomal nanoparticles (LNPs),

Escherichia coli (E.coli) polar lipid extract was ordered from Avanti Polar lipids (Alabaster, AL), and chloroform was acquired from Sigma Aldrich (St. Louis, MO). Anti-Asialoglycoprotein receptor 1 (ASGPR1) /HL-1 antibody (ab49355) and Recombinant anti-ACE2 antibody (ab108252) was acquired from Abcam (Cambridge, MA). Anti-NPHS2 (podocin) polyclonal antibody (MBS3013144) was acquired from MyBioSource (San Diego, CA). GFP monoclonal antibody (GF28R) (MA5-15256) and VDR Monoclonal Antibody (9A7) (MA1-710) were obtained from Thermo Fisher (Waltham, MA).

MiRNA mimics (mmu-miR-298-5p (0.38mg/ml), hsa-miR-26a-5p (0.28mg/ml)), and TaqMan™ MicroRNA assay were ordered from Thermo Fisher Scientific (Waltham, MA). Six ml Becton, Dickinson, and Company (BD) (Franklin Lakes, NJ) hematological tubes spray-coated with 1.8 mg/ml of dipotassium ethylene diamine tetraacetic acid (EDTA), and the blood separation agent Histopaque® 1077 Reagent, which is a solution of polysucrose and sodium diatrizoate (1.077g/mL), was obtained from Sigma-Aldrich (St. Louis, MO). DharmaFECT™ 4 transfection reagent was bought from Horizon Discovery (Cambridge, UK). The LegendPlex™ 8-panel Th1/Th2 Bio-plex assay kit was obtained from BioLegend (San Diego, CA).

Isolation of extracellular vesicles (EVs)

Approximately 10 ml of human blood were put into EDTA-coated BD hematological tubes to declot them. The PBMCs were isolated as described with some modifications [42]. Five ml of EDTA-treated blood samples were layered onto an equal amount of Histopaque® 1077 Reagent in a 15 ml conical tube. The tube was centrifuged at approximately 400 g (1478 rpm) for 30 minutes and 4ºC in an Eppendorf 5810R centrifuge (Hamburg, Germany), which separated the blood into plasma, PBMC, and

erythrocyte layers. The top plasma layer was removed and discarded. The turbid middle layer of PBMCs was removed and put into a clean 15 ml conical tube. The tube was centrifuged at approximately 450 g (1917 rpm) for 10 minutes at 4°C. The supernatant was carefully removed using a transfer pipette. The resulting PBMC pellet was washed with 5 ml of an isotonic phosphate-buffered saline (PBS) (137 mM NaCl, 2 mM KCl, 10 mM Na_2HPO4, 1.8 mM KH_2PO4) solution and centrifuged twice at 300 g (1278 rpm). This pellet was suspended in RPMI growth media without glutamine and phenol red (Corning, NY, USA [43]) and added a 1M HEPES buffer solution (pH 7.4) to a final concentration of 25 mM HEPES to provide additional buffering capacity for the media. Cells were then transferred to a sterile Cellstar T-75 culture flask with a red filter screw cap containing RPMI (with glutamine and phenol red) supplemented with 10% FBS and penicillin/streptomycin. This solution was incubated for about ~12 hours (overnight) in a humidified atmosphere at 37°C and 5% CO_2 in Thermo Fisher Scientific Napco Series 8000 WJ CO_2 incubator (Waltham, MA). Afterward, the media was transferred with a sterilized transfer pipette into 2 ml microcentrifuge tubes. The microcentrifuge tubes were centrifuged at 10,000 g (~14,000 rpm) for 5 min. on a tabletop centrifuge at room temperature. About 1 ml of supernatant from each microcentrifuge tube was transferred to a new 2 ml microcentrifuge tube. Four hundred microliters of precipitation buffer B from the Qiagen (Formerly, Exiqon) miRCURY Exosome Isolation Kit (Qiagen, Germantown, MD) was added to the supernatant in each tube. The microcentrifuge tubes were inverted and vortexed and allowed to incubate for ~12 hours (overnight) at 4°C. The longer incubation time improved the EVs yield from the PBMCs. The remaining steps follow the manufacturer's instructions for the Qiagen miRCURY Exosome Isolation Kit (Qiagen,

Germantown, MD). The EVs were resuspended in 300 µl of the resuspension buffer supplied by the kit, were combined in one tube, and were stored at -80ºC until needed. The total protein concentration of the EVs was measured using the Pierce Bicinchoninic Acid (BCA) Protein Assay Kit (Thermo Fisher Scientific, Waltham, MA) to estimate the concentration and the yield, which was typically around ~10µg.

Preparation of liposomal nanoparticles (LNPs)

Unilamellar liposomal nanoparticles (LNPs) were prepared using the filter extrusion method [44]. The LNPs were comprised of 80% w/v *E. coli* Avanti polar lipids with a defined lipid profile and 20% w/v cholesterol as described previously [45]. Briefly, lipids and cholesterol were mixed in 10 ml chloroform to get a final concentration of 10 mg/ml. This solution was evaporated to dryness in a Rotavapor Model R-114 (Buchi). After evaporation, the film was reconstituted in 0.1 mM EGTA and 50 mM Tris/HCl. This suspension was freeze-thawed at least ten times using liquid nitrogen and extruded 11 times through a LIPEX extruder (Northern Lipids) with a 400 nm cutoff Millipore filter (EMD Millipore).

Functionalized vesicles produced by the "Functionalized Lipid Insertion Method"

The 200 µl solution isotonic PBS solution had a 100 µM of fluorescent NBD-DSPE, a 100 µM of DSPE-PEG2000-maleimide and 0.1% w/v DDM detergent (10X the critical micelle concentration (CMC)). This mixture of components will be referred to as the fatty acid (FA) solution. The NBD-DSPE fluorescence was monitored at 550 nm by exciting at 445-460 nm using a SpectraMax M2 Plate Reader (Molecular Devices, Sunnyvale, CA) to track FA insertion to monitor EVs and LNPs assembly. The FA solution was dialyzed using 0.5 mL Slide-A-Lyzer MINI Dialysis units with a 10 KD cut-off filter (Thermo Fisher

Scientific, Waltham, MA) against 2L isotonic PBS for 2 h at 4°C to remove excess DDM detergent. Almost identical fluorescence for the NBD-DSPE FA was measured after dialysis showing that the lipids remained in solution (data not shown). To ensure that all DSPE-PEG2000 maleimide were conjugated, two-fold excess of the targeting antibody (~200 μM) was added to the dialyzed FA solution and incubated at room temperature for 1 hour. A 100 µl of purified 10 mg/ml EVs or LNPs was added to this 200 µl of the NBD-DSPE, and DSPE-PEG2000-Antibody solution was briefly centrifuged to remove any large aggregates. The molar ratio of vesicle lipid to NBD-DPSE and DSPE-PEG2000-Ab was approximately 75:1:1. This 300 μl solution was incubated for 1 hour at room temperature to allow slow mixing and prevent any potential disruption of the vesicles. After incubation, the supernatant was dialyzed in a 0.5 mL 10 KD cut-off Slide-A-Lyzer MINI Dialysis unit against 2 L of isotonic PBS buffer for two hours at 4°C. Dialysis slowly removes DDM detergent that is surrounding and solubilizing the FAs. The dialysis process exposes hydrophobic surfaces of the derivatized or functionalized FA and entropically drives the FA into the vesicle bilayer to minimize exposure to water to form the functionalized vesicle. The inserted lipids, particularly the DSPE-PEG2000-Ab, remain embedded on the outer leaflet of the vesicle bilayer because a large thermodynamic barrier prevents them from flip-flopping to the inner leaflet [46]. A similar procedure has been used for directionally inserting a membrane protein transporter into a liposome bilayer [52,53]. The orientation was confirmed enzymatically and through atomic force microscopy (AFM) [52,53]. Afterward, the mEV solution was incubated with 100 µl of precipitation buffer B from the Qiagen miRCURY Exosome Isolation Kit (Qiagen, Germantown, MD) for ~12 hours (overnight) at 4 °C (Final volume = ~250 ml), and the

mLNPs solution was centrifuged at 14,000 rpm for 30 minutes to produce a pellet. To pellet the mEVs, the solution was centrifuged at 104,000 g (30,472 rpm) in a Beckman TLA 110 rotor for one hour at 20ºC in a Beckman TLX ultracentrifuge. The supernatant was carefully removed, and the functionalized vesicle pellet was resuspended in 100 μl of isotonic PBS, which will be called the functionalized vesicle solution. The purpose of centrifuging the functionalized vesicles and removing the supernatant is to remove any remaining antibodies that were not cross-linked to the DPSE-PEG2000-Maleimide FA. The concentration of mEVs was measured by protein quantification using Pierce Bicinchoninic Acid (BCA) assay. The concentration of mLNPs was determined by tracking the amount of the lipid that was used throughout the experiments.

Functionalized vesicles produced by the "Detergent-Dialysis Method."

The production of modified vesicles by the "Detergent-Dialysis Method" was done as previously described [17–24]. All the components, the lipids, the proteins if present, and the derivatized lipids, were dissolved in detergent several times higher than the detergent's CMC [17–24]. These solutions were then extensively dialyzed over many hours to remove the detergent [17–24]. The dialysis-driven detergent removal process causes the lipids, the proteins, and the derivatized lipids to randomly coalesce into modified vesicles of indeterminate sizes [17–24]. Differences between this method and the "Functionalized Lipid Insertion Method" are described in the text and Figures 1 and 2.

Lipids functionalized with antibodies (i.e., FA-PEG2000-Antibody) were made as described above. About a milligram of the following mixtures was dissolved in 0.03% DDM, similar to the procedure described in [17]. 1) *E. coli* Avanti polar lipids, 2) *E. coli* Avanti lipids, NBD-DSPE, and DSPE-PEG2000-Antibody with molar ratios of 75:1:1, 3) PBMC-

derived EVs and 4) PBMC-derived EVs, NBD-DSPE, and DSPE-PEG2000-Antibody with molar ratios of 75:1:1 was detergent-solubilized. These detergent-solubilized solutions in 200 μl microcentrifuge tubes were sonicated in a Kendal ultrasonic cleaner HB23 (Kendal) at 25°C until the solutions clarified, indicating complete dissolution. The mixtures were then extensively dialyzed as described in [17] by putting 50 μl of them into 0.2 mL Slide-A-Lyzer MINI Dialysis units with a 10 KD cut-off filter (Thermo Fisher Scientific, Waltham, MA) against 2 L isotonic PBS for at least 45 hours at room temperature.

Characterizing functionalized vesicles

Dynamic light scattering (DLS) was used to characterize the sizes of unmodified and modified vesicles by the "Detergent-Dialysis Method" and the "Functionalized Lipid Insertion Method" (Figure 3), which is well established for this purpose [47–51]. Before the DLS experiments, all the samples were centrifuged at ~8000 g (5,000 rpm) for 30 min. using a Microfuge™ 22R (Beckman Coulter, Brea, CA) at 4°C. The purpose of the centrifugation was to remove large particulates such as dust from the samples, which can interfere with the measurement. Although not visible by the naked eye, all centrifuged samples were assumed to have a pellet, so only the top portion was analyzed by this method. The DLS experiments were performed on a Malvern Zetasizer Nano ZS (Malvern Panalytical, Malvern, UK) using a Malvern 45 μl ultra-micro cuvette (ZEN2112). The DLS experiments were analyzed using the Zetasizer Software Version 8 (Malvern Panalytical, Worcestershire, United Kingdom), assuming a refractive index of 1.330 and a viscosity of 0.8872, which are parameters typically used for lipid-containing vesicles [52]. The size distribution curves in this manuscript were rendered on Igor Pro 6.3 (WaveMetrics, Portland, OR). Protein concentrations of the EVs were determined using Pierce Bis-

cinchonic assay kit (BCA), and LNPs were determined by tracking the lipid concentration throughout the experiments.

Loading functionalized vesicles with miRNA

Electroporation was used to load miRNA in the vesicles, as it is an efficient method to load oligonucleotides into vesicles [48,53]. Equal amounts of mEVs or mLNPs were added with an equal amount of miRNA mimics (Thermo Fisher, Waltham, MA) in SFM for a total volume of 400 μl. The solution was put into 0.4 cm gap Bio-Rad (Hercules, CA) electroporation cuvettes. The miRNA in the *in-vitro* experiments with HepG2 cells varied between 1 and 4 μg, while the miRNA varied between 80 and 110 μg for the *in-vivo* mouse experiments. Unmodified and modified vesicles were electroporated at 150 V and 10-15 ms with an exponential wave pulse in a Bio-Rad Gene Pulser X-Cell electroporator (Hercules, CA). Afterward, the samples were incubated at room temperature and at 4°C for 30 minutes to allow the vesicles to recover.

miRNA delivery to HepG2 cells by functionalized vesicles

Cells were exposed to various combinations of miRNA, vesicles, and modified vesicles to determine their uptake of miRNA. The cells were counted using a hemocytometer on a Zeiss Invertoskop 40 C inverted microscope (Zeiss, Oberkochen, Germany). The cells were plated to approximately 200,000 cells per well in a 6-well VWR tissue culture-treated plates (VWR, Suwanee, GA) and incubated ~12 hours (overnight). Afterward, the media was replenished with 2.7 mL of fresh 10% Eagle's minimal essential medium (EMEM) media. The cells were also fetal bovine serum (FBS)-starved for ~12 hours before treatment to make proliferating cells behave homogenously [54]. For experiments with unmodified and modified vesicles, 400 μl of them were electroporated

with ~4 μg miRNA and then they were added wells in the cell-containing 6-well plates. For the DharmaFECT™ 4 transfection reagent experiments, the reagent was added with ~4 μg miRNA in a 400 μl solution and they were added to other wells in the cell-containing 6-well plates. The final volume for all the wells after adding the solutions was approximately 3 ml. Before RNA extraction, the treated plates were incubated for 72 hours under humidifying conditions at 37°C with 5% CO_2 in a Thermo Fisher Scientific Napco Series 8000 WJ CO_2 incubator (Thermo Fisher, Waltham, MA).

RNA extraction and quantitative RT-PCR (qRT-PCR)

TRIzol Reagent (Invitrogen, Carlsbad, CA) was used to isolate intracellular RNA as per the manufacturer's protocol. All the isolated RNA was stored at -80ºC. Complementary DNA (cDNA) was prepared from intracellular RNA (i.e., microRNA and the housekeeping U6 small nuclear (snRNA)) using the TaqMan™ microRNA Reverse Transcription Kit (Thermo Fisher Scientific, Waltham, MA). The cDNA was analyzed on an Applied Biosystems 7900HT Fast Real-Time PCR System (Applied Biosystems, Foster City, CA) in a 384-well microplate with the TaqMan™ Universal PCR MasterMix (Thermo Fisher Scientific, Waltham, MA). For measurements of miRNA transfer efficiency, TaqMan™ MicroRNA assay (Thermo Fisher Scientific, Waltham, MA) kits with specific fluorescent cDNA primers for the miRNA and fluorescent cDNA primers for the U6 snRNA reference. The DNA was quantitated on the qRT-PCR instrument using the threshold cycle (C_T) method with the U6 snRNA gene as a reference to calculate $\Delta\Delta C_T$ values, which correlates to the relative miRNA uptake [55–58]. These values were exported into Microsoft Excel format to calculate fold difference and analyzed in GraphPad Prism 7

(GraphPad, San Diego, CA). The $\Delta\Delta C_T$ values were normalized against a condition of interest indicate the relative amount of miRNA delivered to the cells.

In-vitro time course for miRNA uptake

Six-well VWR culture-treated plates (Suwanee, GA) were plated with HepG2 cells at a density of 100,000 cells/well. The HepG2 cells were counted using a hemocytometer on a Zeiss Invertoskop 40 C inverted microscope (Zeiss, Oberkochen, Germany). After the cells adhered, the cells were serum-starved for one day. The next day, the cells were treated with functionalized vesicles containing ~4 μg of mmu-miR-298-5p. Before extracting RNA, the cells were incubated from 12 to 72 hrs in a humid atmosphere at 37°C with 5% CO_2 in a Thermo Fisher Scientific Napco Series 8000 WJ CO2 incubator (Waltham, MA). Then, the RNA was extracted and analyzed by qRT-PCR using the procedures described above.

Effect on wound healing by the miRNA delivered by the functionalized vesicles

For quantifying the functional effect of miRNA delivered by mEVs and mLNPs, the modified vesicles were loaded with a tumor suppressor miRNA, miR-26a-5p [47,48]. The HepG2 cells were plated in a 24-well plate at a cell density of 300,000 cells/well. A wound was created in each well using a 200 μl pipette tip followed by subsequent gentle washing with PBS buffer. The cells were then treated with mEVs and mLNPs containing miR-26a-5p at a dosage of 0.35 mg per well (50 ml/well) in 500 ml fresh 10% EMEM media and incubated for 72 hours. The controls for this experiment were untreated cells, cells treated with empty EVs, cells treated with empty mEVs($ASGR1_{PAB}$) under similar conditions. The cells were imaged from 0 to 72 hours on an Olympus IX71 inverted Microscope with a TH4-100 power source (Tokyo, Japan). Untreated HEPG2 cells were used as a control.

The images were analyzed using the Fiji image processing software, an MRI wound healing tool in ImageJ Software (National Institutes of Health, Rockville, MD).

Animal Studies

Eighteen Nu/Nu male nude mice, 48 Nu/Nu female nude mice for targeting studies, and 18 female C57/BL6 mice for immune reactivity studies were ordered from Jackson labs (Maine, USA). All mice were intraperitoneally (IP) injected with a 25-gauge needle and 200 μl or 400 μl of solutions containing SFM or functionalized vesicles in SFM. Unless otherwise specified, each of the functionalized vesicles had 114 μg of mmu-miR-298 microRNA. All the mice were anesthetized using isoflurane (Millipore Sigma, Burlington, MA).

As a negative control, mEVs and mLNPs were bioengineered with the GFP monoclonal antibody ($GF28R_{MAB}$) since they are not known to interact with any mouse proteins (Figure 7). The functionalized vesicles are abbreviated mEV($GF28R_{MAB}$) and mLNP($GF28R_{MAB}$) to denote their modifications. In the experiment, 12 male Nu/Nu nude mice aged 5-7 weeks were divided into three groups (n=3). One group of mice were IP-administered 200 μl of SFM. The next two groups were IP-administered 200 μl mEVs($GF28R_{MAB}$) and mLNPs($GF28R_{MAB}$) electroporated with miRNA (i.e., mmu-miR-298). These functionalized vesicles are abbreviated mEV($GF28R_{MAB}$, mmu-miR-298) and mLNP($GF28R_{MAB}$, mmu-miR-298) to denote their modifications and their miRNA cargo.

The targeting ability against the endocytotic liver ASGR1 receptor was tested with mLNPs and mEVs bioengineered with the ASGR1 polyclonal antibody ($ASGR1_{PAB}$) (Figure 8). For experiments involving mEVs($ASGR1_{PAB}$), six Nu/Nu male mice aged 15-17 weeks were randomly divided into two groups (n=3). For the experiments involving

mLNPs(ASGR1$_{PAB}$), 18 Nu/Nu female mice aged 5-8 weeks were divided into three groups (n=6). The mice then received IP injections with a total volume of 400 μl per mouse. The solutions contained SFM only (untreated), mEVs(ASGR1$_{PAB}$, mmu-miR-298), or mLNPs(ASGR1$_{PAB}$, mmu-miR-298).

Functionalized vesicles, mLNPs, and mEVs were bioengineered with the NPHS2 polyclonal antibody abbreviated mLNP(NPHS2$_{PAB}$) and mEV(NPHS2$_{PAB}$), which targets the kidney-related NPHS2 integral membrane protein (Fig. 9). Six Nu/Nu female mice, aged 5-8 weeks, were divided into two groups (n=3). These mice were IP administered 400 μl containing SFM only, mEVs(NPHS2$_{PAB}$, mmu-miR-298) or mLNPs(NPHS2$_{PAB}$, mmu-miR-298).

Functionalized vesicles, mEVs, and mLNPs were bioengineered with the Angiotensin-converting enzyme 2 monoclonal antibody (ACE2$_{MAB}$) against the membrane-associated ACE2 enzyme, which is part of the Renin-angiotensin system that controls blood pressure (Figure 10) [59]. This antibody was chosen to test the immunoreactivity of functionalized vesicles made by our method because ACE2 is expressed in many tissues ensuring direct interaction with them by these vesicles [60]. Eighteen female C57/BL6 mice, aged 5-8 weeks, were divided into three groups (n=6). These groups received 400 μl IP injections of SFM only, mEVs(ACE2$_{MAB}$, mmu-miR-298), mLNPs(ACE2$_{MAB}$, mmu-miR-298).

***In-vivo* Quantification of miRNA**

After 72 hours, the mice were euthanized using carbon dioxide [61]. After euthanasia, mouse necropsy was performed. Approximately 100 mg sections of each tissue were obtained to assess the amount of miRNA delivered. The sections were

suspended in 1 ml TRIzol reagent (Invitrogen, Carlsbad, CA, USA) in a 1.5 ml microcentrifuge tube. The tissues were homogenized with a 1000 µl digital pipette and a Bel-Art™ Pro Culture Cordless Homogenizer Unit (Thermo Fisher, Waltham, MA). The samples were then centrifuged at 12000 g for five minutes at 4ºC to remove tissue debris with a Microfuge™ 22R centrifuge (Beckman Coulter, Brea, CA). The RNA was extracted using the Invitrogen PureLink™ RNA Mini Kit (Thermo Fisher, Waltham, MA) [62]. After RNA extraction, the RNA concentration was quantified using NanoDrop™ 2000/2000c Spectrophotometer (Thermo Fisher Scientific, Waltham, MA). The RNA concentration was determined using the extinction coefficient for single-stranded RNA in the spectrophotometer of 0.025 $(\mu g/ml)^{-1}$ cm^{-1}, and the RNA purity (>99%) by the 260 nm/280 nm ratio. MiRNA delivered and the housekeeping U6 snRNA, the endogenous control, was quantified using the TaqMan™ microRNA reverse transcription and the TaqMan™ Universal PCR MasterMix (Thermo Fisher Scientific, Waltham, MA) as explained above.

Cytokine assay to probe immunogenicity

In addition to physically observing the mice, a cytokine assay was conducted to determine if the mice elicit an immune response after modified vesicle treatment. Around 1 ml of blood was withdrawn immediately after euthanizing the animals in BD Microtainer® tubes containing serum separator (SST™) (Becton, Dickinson and Company, Franklin Lakes, NJ). The blood was allowed to clot at room temperature for 30 minutes. The tubes were then centrifuged at 1000 g for 15 minutes at 4°C using a Microfuge™ 22R (Beckman Coulter, Brea, CA), and the serum was then stored at -80°C. Before performing the assay, the serum was centrifuge at 10,000 g for 10 minutes at 4°C using a Microfuge™ 22R. The cytokine assay was conducted using Bio-plex Pro™ Mouse cytokine Th1/Th2 assay

kit following the manufacturer's protocols (Bio-Rad, Hercules, CA) [63]. The kit has immunoassays coupled to magnetic beads for detecting the following eight inflammatory factors, including the granulocyte-macrophage colony-stimulating factor (GM-CSF), interferon γ (IFN-g), tumor necrosis factor α (TNF-a), and several interleukins (IL), IL-2, IL-4, IL-5, IL-10, IL-12 (p70). The plate was then read using a Luminex Magpix system (Luminex, Austin, TX).

Statistics

One-way analysis of variance (ANOVA) tests was used to determine statistical significance between groups comparing relative miRNA expression. A confidence interval of 95% with all p-values less than 0.05 were considered significant (*). Student's T-Test was also used to compare two groups, with a 95% confidence interval. Data were analyzed with Microsoft Excel (Microsoft, Redmond, WA) and GraphPad Prism 7 (GraphPad, San Diego, CA).

Results

Methods for producing functionalized vesicles

This work describes a novel method for producing functionalized vesicles involving detergent and dialysis that we called the "Functionalized Lipid Insertion Method." This method is distinct from the "Detergent-Dialysis Method" used for decades and described in the literature since the early 1980s [17–24].

The two approaches are shown schematically in Fig. 1. In the "Detergent-Dialysis Method" (Figs. 1A-B), all functionalized vesicle components are solubilized at a relatively high detergent concentration (Step 1) [e.g., 17,24]. The detergent-solubilized mixture must be extensively dialyzed over many hours or days (Step 2). As dialysis removes the detergent, the vesicles randomly form functionalized vesicles from the solubilized

components. The size of the functionalized vesicle likely depends on the composition of the original components. During the process, the functionalized lipids in the mixture will randomly orient toward the inside and outside the vesicle (red arrows near Step 3). However, even the long dialysis period is not enough to remove all the unintegrated components. Therefore, column chromatography is often needed in addition to dialysis to remove contaminants that interfere with the functionalized vesicle (Step 3) [e.g., 17].

Fig. 1B shows the production of an mEV by the "Detergent-Dialysis Method." A natural vesicle such as an EV must be lysed into its components to be detergent-solubilized as in [19] (Step 1). This process will disrupt its original structure and likely some of its natural functions. Next, the natural vesicle's components, including lipids and proteins, and the functionalized lipid are dissolved at a high detergent concentration (Step 2). This detergent solubilization stage is followed by a long period of dialysis (Step 3) and may require column chromatography (Step 4). The mEV is quite different than the original EV because its natural components randomly reassemble to form it. Both proteins (green arrows) and functionalized lipids (red arrows) assume random orientations within the mEV. Outward-facing proteins are now inward-facing proteins by this approach. Some functionalized lipids are facing inside the vesicle cavity where they cannot perform their intended function.

A graphical representation of the "Functionalized Lipid Insertion Method" discussed in this work is shown in Figs. 1C-1D. The only component that is detergent-solubilized by this approach is the functionalized lipid. In the diagram, the reactive lipid (i.e., DPSE-PEG2000-Maliemide) is solubilized by detergent and dialyzed for two hours to remove excess detergent (Step 1). The purpose of eliminating the excess detergent is

to prevent it from dissolving the target vesicle. Then the detergent-solubilized reactive lipid is incubated for 1 hour with an excess of a targeting component like an antibody (Ab) to allow cross-linking between them (Step 2). Afterward, the functionalized lipid is incubated for another hour with a preformed artificial vesicle or a natural vesicle (Step 3). This incubation period allows the components to slowly combine without external perturbation that might disrupt the vesicles like sonication. Finally, the detergent bound to the functionalized lipid is removed by 2 hours of dialysis (Step 4). A lot less detergent is present, so the dialysis period is significantly shortened. Also, the relatively low detergent concentration reduces the risk that excess detergent will disrupt the target vesicle. Detergent removal from the functionalized lipid exposes hydrophobic parts of the molecule. The functionalized lipid inserts itself into the target into the vesicle in an entropic process to reduce exposure to these hydrophobic surfaces. The FA tail of the functionalized lipid will insert into the target vesicle from the outside. Naturally, the functionalized part of the lipid, which is on the other side of the molecule (red arrowhead), will be facing outward (Step 4). We have already experimentally demonstrated that we can orient membrane proteins in lipid bilayers using a similar principle [52,53].

Possible mechanisms for functionalized vesicle endocytosis and miRNA delivery

The general theory for delivering molecules to a cell is that a targeting molecule on the functionalized vesicle will bind to a surface receptor or excreted receptor ligand. The vesicular uptake can occur by fusion or by several potential endocytosis mechanisms [64]. The specific mechanism of vesicular uptake has not been entirely resolved but appears to be cell-dependent [64].

Fig. 2 shows the potential mechanisms that a functionalized vesicle can be endocytosed by a target cell. The figure shows the binding of the PEG-linked Ab on the functionalized vesicle to a surface receptor on the cell (Step 1). The functionalized vesicle can bind to the receptor and induce endocytosis. Alternatively, the proximity of the functionalized vesicle to the plasma membrane may induce endocytosis with the assistance of a PEG linker (Step 2). Endocytosis of the receptor-bound vesicles leads to an invagination of the cell surface and eventually to the formation of an endosome (Step 3). The endosome eventually disintegrates intracellularly to release the miRNA or other cargo inside the cell (Step 4).

The bottom of Fig. 2 shows the targeting of secretory receptor ligands from cells by functionalized vesicles containing miRNA. In Step 1, soluble proteins are trafficked to the Golgi apparatus from the endoplasmic reticulum (ER) [65]. The Golgi apparatus produces secretory vesicles containing the receptor ligands that migrate to the plasma membrane [65]. At the plasma membrane, they are secreted into the extracellular space, where they are bound by a functionalized vesicle (Step 1) [65]. The functionalized vesicle bound-receptor ligands bind to cell surface receptors on the plasma membrane forms a ternary complex with the receptor. Receptor-ligand binding to the surface receptor induces conformational changes that lead to endocytosis (Step 2) [e.g., 66]. The functionalized vesicle is tethered to the receptor-ligand and surface receptor by a PEG linker allowing the functionalized vesicle to interact with the plasma membrane surface. Interaction of the functionalized vesicle with the plasma membrane can lead to endocytosis. In either case, the functionalized vesicle will be engulfed by the cell to form an endosome (Step 3) [64]. The endosome containing the functionalized vesicle loaded

with miRNA migrates within the cell (Step 3). Eventually, the endosome and the vesicle disintegrate, releasing the miRNA or other cargo intracellularly (Step 4).

The dynamic light scattering (DLS) technique reveals how different processes affect vesicle size

The DLS technique is a well-established technique for estimating particle sizes based on their dynamic scattering properties [67]. The technique has been used extensively to estimate particle size distributions [e.g., 50,68]. The DLS technique was used to determine the effects of the "Detergent-Dialysis Method" and the "Functionalized-Lipid Insertion Method" on the vesicular size distributions. Because functionalized vesicles are assembled all at once with the "Detergent-Dialysis Method," we hypothesize that the initial components of the detergent-solubilized mixture will strongly influence the vesicular size distribution.

Fig. 3 shows DLS measurements of functionalized vesicles produced by the two methods. The predominant particle sizes were determined in each solution by comparing the particle size distribution (PSD) to the diameter in nm. Fig. 3A shows the predominate DDM micelle size (solid line) and a detergent-solubilized NBD-DSPE or DPSE-PEG2000-maleimide micelle size (dotted line) present in solution. The DDM micelle was 6.8 ± 1.6 nm in diameter, while the detergent-solubilized FAs were slightly smaller at 5.7 ± 1.4 nm, consistent with the sizes you would expect for these molecules.

Figs. 3B and 3C show vesicles produced using the "Detergent-Dialysis Method." In Fig. 3B, the LNP (solid line) had an average diameter of 87.8 ± 34.7 nm, similar to previous observations [20]. However, surprisingly, the mLNP (dotted line) had half the diameter of the LNP at 51.2 ± 19.5 nm. This size difference suggests that the size of LNPs

may be sensitive to their lipid compositions, as we hypothesized. Figure 3C shows the EVs (solid line) and mEVs (dotted line) produced using the “Detergent-Dialysis Method.” The EVs created using this method had an average size of 19.7 ± 5.6 nm. In contrast, the diameter of mEVs produced by this approach increased 6-fold to 131 ± 64.5 nm showing that the presence of functionalized lipids during dialysis significantly altered its size.

Fig. 3D and Fig. 3E show the unmodified vesicles and modified vesicles produced using the “Functionalized-Lipid Insertion Method” described in this manuscript. Fig. 3D shows the average particle size of LNPs that are unmodified (solid line). They have an average diameter of 115.6 ± 35.0 nm. LNPs modified using the “Functionalized-Lipid Insertion Method” (dotted line) increased a little over 30% to 160.3 ± 37.4 nm. A 40 nm diameter increase is consistent with the length of the PEG2000 linker connecting to an Ab of the mLNP [69,70]. The unmodified EVs shown in Fig. 3E (solid line) were 21.2 ± 5.9 nm, which is similar to the EV sizes produced with the “Detergent-Dialysis Method” (Fig. 3C, dotted line). In Figure 3E (dotted line), the EVs increased only 17% or 5 nm to 24.7 ± 6.9 nm. The size increase for mEVs was relatively modest for functionalized vesicles created by this method, suggesting that their original structures were intact. One possibility is that the plasma membranes of EVs are crowded with many intrinsic membrane proteins that interfere with functionalized lipid insertion [e.g., 71]. The other possibility is geometrical. Because mEVs are smaller than mLNPs, their surface areas will be much larger within a given volume than mLNPs. In other words, a lot more functionalized lipids will be required to have the same density on mEVs than mLNPs.

In-vitro delivery of miRNA by functionalized vesicles produced from the “Functionalized-Lipid Insertion Method”

The human liver HepG2 cancer cell line has been the focus of many *in vitro* studies related to the functioning of liver cells and liver cancer [72–74]. The endocytotic asialoglycoprotein receptor 1 (ASGR1) is highly expressed on the surface of HEPG2 cells [75]. The endocytotic process involves receptor-ligand binding and ASGR1 trimerization through receptor-mediated endocytosis [76]. This receptor has already been exploited to mediate small molecule uptake into HepG2 cells [77–79]. For example, galactosamine-linked to albumin and nanoparticles loaded with pullulan and arabinogalactan delivered the anti-cancer drug doxorubicin to HepG2 cancer cells [77,78]. In another study, pegylated liposomes modified with lactoferrin successfully delivered the fluorophore coumarin-6 to the ASGR1 receptor on isolated HepG2 cells and HepG2 cells implanted in nude mice [79]. Finally, antisense oligonucleotides have been delivered to HepG2 cells by linking to the ASGR1 substrate *N*-acetylgalactosamine [80]. As far as we know, ASGR1 Abs have never been used to facilitate molecular uptake through the ASGR1 receptor with HepG2 cells. In this study, modified vesicles were made with a polyclonal antibody for the ASGR1 receptor ($ASGR1_{PAB}$), which targets the EC domain of the ASGR1 receptor.

Initially, we wanted a miRNA that could modulate the expression of the multi-drug resistance (MDR) transporter (a.k.a. P-glycoprotein or P-gp), which is the focus of my lab and research funding. With the functionalized vesicles, we were interested in modulating *in vivo* and *in vitro* expression of P-gp. Our former collaborator, who is an expert in miRNA, recommended that we investigate mouse miR-298 based on the following papers with miR-298 [81,82]. The miR-298 in [81] turned out to be human miRNA-298, which has an

entirely different sequence and function than mouse miRNA-298 [83]. That revelation was one of the primary reasons for ending our collaboration.

The mouse miR-298 is also known as mmu-miR-298-5p, where mmu reflects the species Mus musculus (house mouse), the number is sequentially determined, and 5p refers to the 5' side of the miR-298 stem-loop [81]. As far as we know, this miRNA is not known to affect the expression of human genes, and human cells are not known to express it. Therefore, the mmu-miR-298-5p was used as a probe miRNA.

Fig. 4 are experiments to estimate the relative uptake of mmu-miR-298-5p in HepG2 cells. The experiments shown in Fig. 4A were used to gauge the uptake of ~4 μg of mmu-miR-298-5p into the HepG2 cell line using various treatments. The relative uptake of mmu-miR-298-5p was normalized against HepG2 cells treated with DharmaFect 4 transfection reagent with ~4 μg miRNA abbreviated DharmaFect(miRNA). No mmu-miR-298-5p was detected in untreated HepG2 cells. HepG2 cells treated with EVs electroporated with mmu-miR-298-5p (abbreviated EVs(miRNA)) had miRNA uptake efficiency that was 5-fold higher than HepG2 cells treated with DharmaFect(miRNA). The miRNA uptake efficiency of HepG2 with EVs constructed with the $ASGR1_{PAB}$ and loaded with mmu-miR-298-5p (abbreviated mEVs($ASGR1_{PAB}$, miRNA) showed 8-fold greater improvement in miRNA uptake than DharmaFect(miRNA) control. HepG2 cells treated with exosomes genetically engineered with an Apolipoprotein A1 targeting ligand had more efficient miRNA uptake [48]. We hypothesize that the Apolipoprotein A1 targeting ligand on the exosome works better with the endocytotic mechanism of the ASGR1 receptor than the $ASGR1_{PAB}$ that targets different parts of the EC domains [76]. Also,

internalization through the Apolipoprotein A1 targeting ligand only requires binding to the scavenger receptor, class B, type I (SR-BI) to initiate endocytosis [76,84,85].

Modified LNPs with $ASGR1_{PAB}$ were also made and loaded with ~4 μg mmu-miR-298 (abbreviated mLNP($ASGR1_{PAB}$, miRNA)). Fig. 4B shows the relative miRNA uptake by HepG2 cells treated with mLNPs($ASGR1_{PAB}$, miRNA) and treated with mEVs($ASGR1_{PAB}$, miRNA). The overall miRNA uptake was normalized against HepG2 cells treated with DharmaFECT(miRNA). Relative miRNA uptake was almost 2-fold higher in HepG2 cells treated with mLNPs ($ASGR1_{PAB}$, miRNA) than cells treated with mEVs ($ASGR1_{PAB}$, miRNA). The higher miRNA uptake by HepG2 cells treated with mLNPs may be the result of more functionalized lipids or more miRNA per vesicle because of their relative size (cf. Figures 3D and 3E).

The miRNA uptake's temporal efficiency depends on the miRNA endocytotic mechanism, the miRNA carrier vehicle, and the miRNA type [86,87]. For example, the miRNA uptake of a human ovarian cancer cell line treated with liposomes loaded with fluorescently-labeled hsa-miR-7-5p increased linearly over 24 hours [86]. The uptake of miRNA in multiple myeloma treated with stable nucleic acid-lipid particles (SNALPs) loaded with hsa-miR-34a decreased after 48 hours [87]. In this study, the miRNA uptake in HepG2 cells after treatment with mLNP($ASGR1_{PAB}$, miRNA) and mEV($ASGR1_{PAB}$, mRNA) was examined over 72 hours (Fig. 4C). The uptake efficiency of HepG2 cells to mmu-miR-298-5p increased exponentially by treatment with mLNPs or mEVs. After incubating the cells for 24 hours, the uptake efficiency approximately doubled every 12 hours for the mEVs and 8 hours for the mLNPs. The uptake at 72 hours for mLNPs and mEVs was 600 and 250-fold higher, respectively, above the background in untreated

controls. The 72-hour time frame seemed like a suitable sensitivity for the *in vivo* mice experiments to determine how well the functionalized vesicles target and whether there is significant immunogenicity from the treatment.

Modified vesicles reduce HepG2 cell proliferation by enhancing hsa-miR-26a-5p uptake

The functional effects of treating HepG2 cells were tested with the mEVs(ASGR1$_{PAB}$), and mLNPs(ASGR1$_{PAB}$) loaded with miRNA hsa-miR-26a-5p (abbreviated mEV(ASGR1$_{PAB}$, miRNA) and mLNP(ASGR1$_{PAB}$, miRNA)). The miRNA hsa-miR-26a-5p was chosen to inhibit HepG2 cell proliferation and promote HepG2 cell apoptosis [48]. In other words, the miRNA would slow the closure of wounds made on a layer of HepG2 cells.

Wound healing assays with bright field microscopy have effectively gauged cell proliferation and migration in prior studies [88,89]. The approach was used to gauge the effect of mEVs and mLNPs treatment of HepG2 cells in Fig. 5. Fig. 5A shows the wound closures of HepG2 cells after various treatments at 0 and 72 hours. For untreated cells, the wound closed to about half its original width. The HepG2 cells treated with empty EVs (abbreviated EV()), unmodified extracellular vesicles electroporated with hsa-miR-26a (abbreviated EV(hsa-miR-26a)), and empty modified extracellular vesicles with the polyclonal antibody for the ASGR1 receptor (abbreviated mEV(ASGR1$_{PAB}$)) had an almost similar extent of wound closure as the untreated cells meaning no effect on cell proliferation. The wound area for HepG2 cells after treatment with mEVs(ASGR1$_{PAB}$, miRNA) and mLNPs(ASGR1$_{PAB}$, miRNA) almost completely inhibited wound closure, demonstrating efficient uptake of hsa-miR-26a.

This wound closure over 72 hours was assessed quantitatively in Fig. 5B. The percent wound closure by all the treatment groups was normalized to the amount of wound healing in the untreated cells. The results show that the relative amount of wound closure in the cells treated with empty EVs, EVs(hsa-miR-26a), and mEVs(ASGR1$_{PAB}$) was virtually identical to untreated cells. For EVs(hsa-miR-26a), the lack of effect on cell proliferation may be due to inefficient uptake of the hsa-miR-26a miRNA by the HepG2 cells. In contrast, wound closure by cells treated with mEVs(ASGR1$_{PAB}$, hsa-miR-26a) or mLNPs(ASGR1$_{PAB}$, hsa-miR-26a) inhibited cell proliferation by 50%.

Along with wound closure, the relative wound area was also analyzed for three-time points, as shown in Fig. 5C. The wound in untreated HepG2 cells closed at 16 ± 3 % per day (open circles). This wound closure rate is close to the 19% per day observed for HepG2 treated with extracellular vesicles containing hsa-miR-26a (calculated from Fig. 5B in [48]). After three days, the wound area was reduced to 52 ± 8% of the original area, indicating uninhibited cell proliferation. The relative wound area in the cells treated with EVs delivering miRNA (abbreviated EVs(miRNA), open squares) was reduced at the rate of 13.9 ± 1.5 % per day, thus not differing significantly from untreated cells. Treating the HepG2 cells with mEVs(ASGR1$_{PAB}$, miRNA) decreased the rate of closure to 5 ± 4.3% per day (closed circles) and with mLNPs(ASGR1$_{PAB}$, miRNA) decreased the rate of closure to 6.7 ± 1.8% per day (closed squares). HepG2 cells treated with either our mEVs or mLNPs inhibited cell proliferation better than HepG2 cell treatment with miRNA-loaded Apo A1 targeting ligand exosomes, which only decreased cellular proliferation to 10% per day (calculated from Fig. 5B in [48]).

Process of *in vivo* targeting of modified vesicles

The uptake of miRNA in mice after treatment with mEVs and mLNPs is shown in Fig. 6. Modified vesicles are loaded with miRNA by electroporation and injected intraperitoneally (IP) into mice (Fig. 6A). Because of their small physical size, IP administration to mice was easier and more reliable than intravenous (IV) administration [90–94]. Also, vesicles administered by IP injection distribute broadly to the organs and the visceral adipose tissue because of the lymphatic system [90–94], which was preferred for testing our modified vesicles.

The treated mice are euthanized after three days using carbon dioxide followed by cervical dislocation, and their organs are harvested (Fig. 6B). The tissue was analyzed using RNA extraction protocols that are described in the *Materials and Methods* (Fig.6C). The relative miRNA concentration taken up in the organs is compared to the relative concentration of the U6 housekeeping gene using primers specific for the miRNA and qRT-PCR (Fig. 6D). The crossover threshold (C_t) is determined for the miRNA and the U6 housekeeping genes. Finally, the relative-fold miRNA uptake in the mouse organs is determined by the $\Delta\Delta C_t$ method (Fig. 6E).

I*n vivo* studies with mmu-miR-298-5p were originally intended to modulate P-gp expression as recommended and suggested by our former collaborator but does not have that function [81,82,95–97]. As far as we are aware, no microRNAs are known to affect mouse P-gp expression or any related mouse transporters within its superfamily. Our former collaborator made miRNA sound specific, especially with respect to P-gp transporter expression, but a single miRNA can have many physiological functions [98]. For example, the mmu-miR-298-5p is known to target the nuclear factor (NF)-κB activator 1 (Act1) involved in cell signaling pathways and autophagy [95,99]. The miRNA is also

known to regulate the expression of β-Amyloid Precursor Protein-converting Enzyme 1 [96] and regulate the expression of the insulin-like growth factor-1 β (IGF1Rβ) [97]. The miRNA also has a wide variety of theoretical targets that remain to be investigated in the TargetScanVert and miRDB databases [100,101]. Therefore, the following *in vivo* experiments with the functionalized vesicles and mice will determine their organ specificity and immunogenicity. Furthermore, siRNAs have already been shown to affect mouse P-gp expression [53,102]. Therefore, functionalized vesicles loaded with the siRNA may be a practical delivery vehicle to investigate the P-gp transporter in the future.

In vivo miRNA delivery by functionalized vesicles with a non-interacting antibody

As a negative control for *in-vivo* targeting ability of mEVs and mLNPs, mice were treated with modified vesicles loaded with miRNA and the rabbit polyclonal green fluorescent protein antibody (GFP_{PAB}) as the non-targeting antibody. Polyclonal antibodies have higher avidity than monoclonal antibodies but can show cross-reactivity to non-target proteins [103]. At least in mice, the GFP_{PAB} (Novus, NB600-308) only targets GFP and no other proteins [104,105]. Fig. 7 shows the uptake of mmu-miR-298 treated with modified vesicles with the GFP_{PAB} and containing mmu-miR-298 (i.e., mEVs(GFP_{PAB}, mmu-miR-298) and mLNPs(GFP_{PAB}, mmu-miR-298)). Significant miRNA uptake in all the organs of mice treated with non-targeting mEVs and mLNPs was within 30% between all the organs that were investigated. This distribution in uptake efficiencies is consistent with the mEVs and mLNPs lacking specific organ targeting ability. The highest miRNA uptake with the modified vesicles was observed in the mouse spleen, which is not surprising considering that it is directly connected to the lymphatic system and is considered a lymphoid organ [106]. The liver had about a third of the miRNA uptake than the spleen.

The kidney and the lungs had only 20% of the miRNA uptake of the liver and 5% of the miRNA uptake of the spleen. Less than 1% of miRNA uptake was observed in the brain. The miRNA uptake in mice follows a very similar pattern for biotin-labeled liposomal uptake in the organs of rats, with the exception of liposomal uptake in the lungs [107].

***In vivo* targeted miRNA delivery to the liver by functionalized vesicles with the ASGR1 antibody**

After successfully delivering miRNAs by both mEVs and mLNPs bioengineered with ASGR1 antibody to hepatocellular carcinoma HepG2 cells (Fig. 4), we wanted to assess the capability of these vehicles in targeting the liver *in vivo* utilizing the same antibody. Mice were treated with mEVs($ASGR1_{PAB}$, mmu-miR-298) and mLNPs($ASGR1_{PAB}$, mmu-miR-298) like the *in vitro* experiments.

Fig. 8 shows the uptake of miRNA by liver, lungs, spleen, kidney, and brain in mice treated with mEVs($ASGR1_{PAB}$, mmu-miR-298) and mEVs($ASGR1_{PAB}$, mmu-miR-298) normalized to the endogenous levels of mmu-miR-298 that is present in mice. MiRNA delivery from both mEVs and mLNPs was almost entirely to the liver while relatively non-significant in other organs. The high specificity for the mEVs and mLNPs to the liver may be due to the target of $ASGR1_{PAB}$ being the ASGR1 receptor, which is naturally endocytotic.

***In vivo* targeted miRNA delivery to the kidney by modified vesicles with the NPHS2 antibody**

NPHS2 (a.k.a. Podocin) is a non-endocytotic protein associated with the kidney [108], so we engineered modified vesicles engineered an NPHS2 polyclonal antibody ($NPHS2_{PAB}$) to see how well it would these vesicles would target the kidney with mmu-

miR-298. Fig. 9A shows the amount of miRNA delivered by mEVs(NPHS2$_{PAB}$, mmu-miR-298) to five major organs: kidney, liver, lungs, spleen, and brain. The amount of miRNA was normalized to the endogenous levels of mmu-miR-298 in mice only treated with SFM. The distribution of microRNA uptake was significantly different than mEVs and mLNPs engineered with the GFP$_{PAB}$ (Fig. 7), suggesting that the NPHS2$_{PAB}$ on the modified vesicles affected the organ targeting. However, these modified vesicles were less specific than mEVs and mLNPs with ASGR1$_{PAB}$ (Fig. 8), which may be because the NPHS2 protein is not naturally endocytotic [108] or cross-reactivity of a polyclonal antibody [109,110]. The mmu-miR-298 delivered to the kidney and spleen was the highest of all the organs and was 125-150 fold higher than untreated mice. Since the spleen is not known to express the NPHS2 protein, the higher spleen uptake is likely due to the route of administration. The lungs and the liver showed significantly less uptake at ~25 fold and ~60 fold, respectively. No significant microRNA uptake was found in the brain. Modified LNPs (abbreviated mLNPs(NPHS2$_{PAB}$, mmu-miR-298) or mLNPs(NPHS2$_{PAB}$, miRNA)) also showed a very similar delivery distribution (Fig. 9B) as mEVs(NPHS2$_{PAB}$, mmu-miR-298), inferring that the NPHS2$_{PAB}$ had similar targeting effects in both of these modified vesicles.

Immunogenic effects of miRNA delivery by modified vesicles with the relatively non-specific ACE2 antibody

To explore the immunogenicity of mEVs and mLNPs in-vivo, a targeting vesicle was engineered with a monoclonal antibody against the membrane-associated angiotensin-converting enzyme 2 (ACE2) (ACE2$_{MAB}$). This enzyme is ubiquitously expressed in many organs throughout the body and plays a crucial role in controlling

blood pressure [60,111–114]. In rodents, ACE2 mRNA levels were highest in the ileum in both mice and rats, followed by the kidney, almost equal levels in the lungs, bladder, stomach, colon, adipose tissue, atrium, brainstem, forebrain, and ventricle [115]. The lowest ACE2 mRNA was in the spleen of the rodents [115]. A different but pervasive pattern in protein levels was observed with the highest in the atrium (124.5%) and ventricle (131.7%), moderate expression in the kidney (100%), lesser in the lung (19.7%), testis (28.7%), thymus (44.4%), and least amount in the spleen [115]. Therefore, targeting mEVs and mLNPs with $ACE2_{MAB}$ will be relatively non-specific but more evenly distributed among the organs than mEVs and mLNPs with GFP_{PAB}, which primarily targeted the spleen (Fig. 7).

Fig. 10 shows the uptake of mmu-miR-298 and their effects on the cytokine levels after treatment of mice with miRNA-loaded mEVs and mLNPs engineered with $ACE2_{MAB}$. In Fig. 10A, the relative miRNA uptake was analyzed in various organs to determine possible immunogenic effects, including the lungs, liver, small intestine, spleen, brain, kidney, and heart. Increased levels of miR-298 were observed in all the analyzed organized versus the mice treated with only SFM. The uptake of miRNA by treatment of mice with mLNPs($ACE2_{MAB}$, mmu-miR-298) was highest for the small intestine (~830 fold) followed by the kidney (~530 fold), spleen (~400 fold), liver (~400 fold), heart (~388 fold), and lungs (~100 fold). Virtually no miRNA uptake was observed in the brains of mice. Except for the spleen, these relative miRNA uptake levels are consistent with the protein expression levels of the ACE2 protein in rodents and humans [60,114,115]. The distribution of miRNA delivery to organs by mEVs($ACE2_{MAB}$, mmu-miR-298) differed significantly from mLNPs. From high to low fold miRNA uptake by mEV treated mice

versus mice treated with SFM only, the miRNA uptake in mice by mEVs was ~280 fold in the liver, ~250 fold in the kidneys, ~200 fold in the spleen, ~200 fold in the lungs, ~90 fold in the small intestine, ~70 fold in the heart and ~25 fold in the brain (Figure 10B). Since there is almost no ACE2 enzyme in the spleen [115], the relatively high miRNA uptake after treatment with mEVs and mLNPs is likely due to the route of administration rather than specific targeting by $ACE2_{MAB}$ of the modified vesicles.

The immunogenicity of the functionalized vesicles was assessed by LegendPlex™ 8-panel Th1/Th2 Bio-plex assay, which tests for 8 major anti- and pro-inflammatory cytokines from two types of CD4+ T helper lymphocytes [116]. Cytokine profiling has been used previously to determine the immunogenicity of EVs and LNPS [117,118]. Fig. 10C shows the cytokine levels in mice treated with mEVs($ACE2_{MAB}$, mmu-miR-298) and mLNPs($ACE2_{MAB}$, mmu-miR-298) in comparison to mice treated with SFM. No statistically significant change in cytokine levels was observed in mice treated with either mEVs or mLNPs. In addition, throughout all the *in vivo* experiments in this study (Figs. 7-10), no physical manifestations of immune response were observed, such as redness, itching, or sudden hair loss.

Discussion

In this work, we present the “Functionalized Lipid Insertion Method” to bioengineer targeting functionalized vesicles with a surface coated with PEG-linked Abs that we referred to as mEVs or mLNPs. We explain how our approach is significantly different from the “Detergent-Dialysis Method” used since the 1980s [17–24]. These functionalized vesicles are versatile and can target surface receptors. Both mEVs and mLNPs could efficiently deliver miRNA to the HEPG2 cell line. The *in-vitro* miRNA uptake efficiency was

8-fold and 15-fold higher than the transfection reagent by mEVs and mLNPs, respectively. mEVs treatment of cells with growth-affecting miRNA caused significant effects on mRNA expression and cellular growth. Targeted delivery of miRNA to the liver (more than 80%) and kidney (more than 50%) was achieved by both mEVs and mLNPs in-vivo. The modified vesicles also were essentially non-immunogenic (Figure 10).

Even unmodified extracellular vesicles can have oligonucleotide uptake efficiencies and target cells like mEVs [119,120]. Exosomes derived from the human hepatoma Huh7 cell line targeted the human embryonic kidney line over human PBMCs or a human lymphoblast cell line [119]. The miRNA uptake efficiencies for the human embryonic kidney cell line treated with exosomes were 5-200-fold higher than the other cell lines [119]. A study with exosomes derived from MDA-MB-231 cells and H-29 colon cancer cells suggested that efficient exosomal targeting relied on complementary interactions [120]. Unmodified exosomes are the simplest to produce but predicting the exosomal target requires analyzing the oligonucleotide uptake in various tissues and cell lines to determine specificity.

Several methods have been developed to modify the surfaces of natural vesicles to control targeting to cells and improve uptake of oligonucleotides [15,53,120]. Targeting and miRNA uptake of CD8+ T-cell-derived exosomes to effector T-cells was enhanced by having a constitutive exosomal protein bound with antibodies [15]. Unfortunately, this simple approach does not have broader applicability to exosomal targeting beyond T-cells. Another strategy to exploit constitutive exosomal proteins is to fuse them with targeting proteins by genetic engineering [121]. Exosomes were genetically engineered with a lysosomal protein (Lamp2b) and the rabies viral glycoprotein (RVG) [72]. They

were able to enhance siRNA uptake efficiency in cells and overcome the blood-brain barrier (BBB) in mice [53]. Exosomes have been genetically engineered using a similar technique with fusion proteins of the lysosomal protein (Lamp2) with the green fluorescent protein (GFP) for fluorescent tracking and with the HER2 affibody for targeting [122]. Exosomes have also been genetically engineered with a construct made from the vesicular stomatitis virus glycoprotein with improved loading, delivery, and tracking [123]. The development of modified exosomes by genetic engineering is limited by the complexity of engineering the fusion protein construct and getting the construct to express in budding exosomes [121].

A highly PEGylated exosome with a relatively low surface density of Abs than Abi-exosomes was developed using a two-stage process to deliver anticancer drugs cells [16]. The modified exosomes provided only a ~30% increase in anticancer drug uptake by a human pancreatic cancer cell line [16].

Similarly, modified and unmodified LNPs have been used to deliver miRNA previously. Cationic liposomes have been used as transfection agents to deliver miRNA such as miR-7 to ovarian cancer cells, miR-143 and -145 in human colorectal tumors, and miR-122 in liver cells achieving up to 80% efficiency [86,124,125]. Cationic liposomes typically consist of a cationic lipid, neutral lipid and/or cholesterol, and a PEG-lipid. Cationic liposomes are known to form ion pairs with anionic phospholipids of the endosomal membrane leading to the release of cargo efficiently, which makes them one of the promising drug delivery vehicles. Cationic liposomes can form complexes with oligonucleotides such as miRNA and are known as lipoplexes. For instance, a cationic-based lipoplex delivery system has been used to deliver miR-29b and miR-133b to non-

small cell lung cancer cells. The lipoplexes achieved over 2-fold delivery efficiency in comparison to the transfection reagent *in vitro*. In addition to low delivery efficiency, when injected intravenously, only 30% accumulation was achieved in the target organ, lungs, with the highest amount found in the liver, followed by kidney and spleen [126,127]. The process of preparing lipoplexes, unfortunately, renders them unoptimizable down the process and increases the risk of interaction of cationic lipids with other tissues making them non-specific, limiting their potential as targeted drug delivery vehicles.

In addition to cationic liposomes, liposomes can also be conjugated with target-specific vectors to design cell-specific vehicles. Targeted liposomes have been prepared by conjugating Aptamer (AS1411), a target-specific single-stranded oligonucleotide, using thioether linkage between DSPE-PEG2000 maleimide on the liposomal surface. These Aptamer functionalized liposomes were used to deliver miR-29b to A2780 cells, ovarian cancer cells [128]. Another study prepared a liposome-polycation-hyaluronic acid (LPH) modified with GC4 single-chain variable fragment, a tumor-targeting monoclonal antibody to deliver siRNA and miRNA to B16F10, metastatic lung cancer cells [129]. The GC4 targeted liposomes achieved 40% delivery of siRNA in the tumor, and the highest accumulation was achieved in the liver (>50%) when dosed intravenously to the tumor-bearing mice [129]. An antibody against the CD59 receptor, a receptor overexpressed in cervical cancers, was conjugated to Cisplatin (CDDP)/miR-1284-loaded liposomes. CD59 conjugated vehicles showed a significant increase in miRNA-induced cytotoxicity in cervical cancer cells and prolonged blood circulation of cisplatin [130]. All these studies have used the post-conjugation method to modify liposomes, where they attach derivatized PEGylated lipids to the liposomes while preparing liposomes followed by

conjugation of antibodies. Although successful, this method is more complicated as you functionalize lipid derivatives even before preparing liposomes. However, the post-insertion method, also known as the detergent dialysis method, attachment of antibodies to derivatized lipids first, and then inserting antibody derivatized lipids in PEGylated liposomes, gives more room to play with designing or modifying liposomes as desired. The Detergent-dialysis method has been shown to be as effective as if not more than the post conjugation method [131]. This method has been used to attach target-specific antibodies such as CD44 and CD133 to deliver cargoes like small molecules like doxorubicin or antibodies like anti-IL6R antibodies [132,133]. However, as mentioned earlier, this method requires extensive dialysis over a long time, increasing the risk of degradation (in the case of natural vesicles), aggregation, and attachment of functionalizing ligands both internally and externally.

Considering the versatility of the “Functionalized Lipid Insertion Method,” the approach seems to be the simplest and most efficient way to modify therapeutic delivery vehicles. Fluorescence tracking, PEGylation, and Ab targeting are integrated into a single dialysis step followed by electroporation for oligonucleotide loading. Many of the pieces for industrial-scale production of mEVs are already available. Industrial methods for dialyzing and electroporation have already been around for decades [134,135]. Synthetic methods are available to produce large amounts of miRNA [136]. Innovative large-scale production of monoclonal Abs is being developed from plants [137]. Currently, getting EVs is rate-limiting, but methods are on the horizon for getting from abundant sources such as milk [138,139]. Liposomes have been around for more than a few decades, with different methods available to upscale their preparation, including microfluidics [140,141].

Several challenges exist for implementing mEVs and mLNPs therapeutically. For long-term viability, EVs and, by extension, mEVs are most often stored at -80ºC. However, month-long room temperature storage has been shown after lyophilization and in the presence of trehalose [41,142]. In contrast, lyophilized LNPs can last up to a year at 4ºC or room temperature in an oxygen-free environment [143–146]. MicroRNAs also have their challenges and must often be stored at -80ºC [147], but methods are available to increase temperature stability through chemical modification [148]. MiRNA also has the potential for slowly leaking from functionalized vesicles [149].

Authors contributions

Authorship was determined using guidelines recommended by *The International Committee of Medical Journal Editors* [150–153], which requires major and novel contributions to scholarship and provided a major role in the organization and intellectual ideas within this manuscript. The original development of the "Functionalized Lipid Insertion Method" was based on membrane protein reconstitution in liposomes previously done in Dr. Arthur G. Roberts laboratory [52,53]. Ms. Pragati Jain made significant improvements to the experimental protocol that was part of Dr. Sudeepti Kuppa's Ph.D. thesis. Ms. Pragati Jain and Dr. Arthur G. Roberts played the largest roles in designing the experiments within the manuscript, as evidenced by their many individual meetings. They both played major roles in the writing and the organization of the manuscript. Ms. Pragati Jain selected the specific antibodies and most of the other materials that were used within the project. Dr. Arthur G. Roberts selected the fluorescent and reactive lipids used in this project and designed the original protocol for functionalized vesicles, as well as contributed to modified versions by Dr. Sudeepti Kuppa and Ms. Pragati Jain. Ms. Pragati Jain did all of the data collection and almost all of the data analysis.

Acknowledgements

We would like to thank the National Cancer Institute Grant (1R01CA204846-01A1) for the resources necessary for this research. We would like to thank the generosity of several Pharmaceutical and Biomedical Sciences (PBS) Department faculty members at the University of Georgia (UGA) for sharing their instrumentation, their cell culture hoods, their animal use protocols (AUPs), and space within the animal facilities at the Davidson Life Sciences and the Coverdell buildings at the University of Georgia, Athens, GA 30602. We greatly appreciate the help that Dr. Charnel Byrnes, who trained Ms. Pragati Jain in extracting PBMCs, trained her in basic mammalian cell culture techniques, and assisted her in optimizing electroporation for loading vesicles with miRNA. We want to thank Drs. Mandi M. Murph and Yao Yao for assistance with the mice experiments. We would also like to thank Dr. Balazs Rada for assisting us in getting PBMCs from human volunteers. We want to thank Dr. Sergiy Minko for providing the DLS machine for vesicle size determination from his laboratory. We would also like to thank various PBS faculty members at the UGA for giving comments and suggestions for this project. Most importantly, we would like to thank Dr. Sudeepti Kuppa, who used the original protocol that I designed and got the method to work *in vitro* in the breast cancer MDA-MB-231 cell line, which was a significant part of her Ph.D. thesis.

Figure Legends.

Figure 1. Bioengineering functionalized vesicles by the "Detergent-Dialysis Method" and the "Functionalized-Lipid Method." A) Shows the "Detergent-Dialysis Method" that has been used since the 1980s to produce functionalized vesicles from LNPs. In Step 1, functionalized lipids containing a targeting molecule such as an Ab are mixed with lipids and high concentrations of detergent, leading to complete solubilization of all the components. In Step 2, the high concentrations of detergent are dialyzed over a long time period to remove the detergent. When enough detergent is removed, the mLNPs will spontaneously form, but the orientations of the functionalized lipids become randomized (red arrows) within the lipid bilayer. Even after this long dialysis period, column chromatography may be required to remove detergent-solubilized components in Step 3. B) Shows the process of using the method to produce functionalized vesicles from natural vesicles like EVs. A key difference with producing mEVs over producing mLNPs is that they must be lysed into their individual components in Step 1 prior to detergent solubilization and dialysis in Steps 2 and 3. In Step 3, Because proteins are likely to be embedded in the natural vesicle lipid bilayer, their orientations will be randomly oriented (green arrows) like the functionalized lipids (red arrows). Column chromatography might be required afterward in Step 4 to remove detergent-solubilized contaminants. C) Shows the process of producing mLNPs using the "Functionalized Lipid Insertion Method." In Step 1, detergent-solubilized lipids with reactive functional groups are dialyzed for two hours to remove excess detergent. These solubilized lipids are mixed with targeting molecules such as Abs for 1 hour to form functionalized lipids in Step 2. In Step 3, the functionalized lipids are then incubated (or mixed gently) with preformed LNPs for another

hour to ensure the integrity of the preformed vesicle. In Step 4, because the detergent concentration is relatively small compared with the detergent concentrations used in the "Detergent-Dialysis Method," a lot shorter time period is required for their removal. Removal of detergent from the functionalized lipids causes them to directionally insert into the preformed liposomes, becoming mLNPs. D) Shows natural vesicles like EVs being produced by the "Functionalized Lipid Insertion Method." The process of producing mEVs is virtually identical to producing mLNPs. In Steps 1 and 2, a detergent-solubilized functionalized lipid is produced from dialysis and incubation with targeting molecules such as Abs. Then in Step 3, they are incubated (or gently mixed) with the EV to maintain vesicle integrity. Detergent removal through dialysis inserts the functionalized lipid directionally into the EV forming an mEV.

Figure 2. Potential mechanisms for cellular endocytosis of functionalized vesicles. A) A functionalized vesicle binds to a cell surface endocytotic receptor in Step 1 and then undergoes endocytosis in Step 2. The receptor-bound functionalized vesicle forms an endosome in Step 3 and eventually disintegrates in Step 4 to release its contents like R. B) A soluble receptor-ligand migrates to the plasma membrane surface from the Golgi apparatus, where it binds to a functionalized vesicle in Step 1. In order for the soluble protein-bound functionalized vesicle to be internalized by a cell, the complex binds to a cell surface receptor forming a ternary complex in step 2. If the surface receptor is endocytotic, the functionalized vesicle-bound receptor ligand is endocytosed to form an endosome in Step 3. Alternatively, if the functionalized vesicle is connected to the receptor-ligand through a long linker like PEG2000, the functionalized vesicle might

contact the plasma surface leading to endocytosis. The resulting endosome disintegrates and releases its contents, such as R in Step 4. Abbreviations: R, miRNA.

Figure 3. Size distribution of functionalized vesicles determined by dynamic light scattering (DLS). A) Detergent DDM micelles (solid line) and DDM-solubilized FAs (dashed line). The "Detergent-Dialysis Method" was used B) to produce the size distributions of LNPs (solid line) and mLNPs (dashed line) and C) to produce the size distributions of EVs (solid line) and mEVs (dashed line). The solid lines in panels D) and E) show the size distributions produced for LNPs using the extrusion approach [44] and EVs through isolation and purification protocols described in the Materials and Methods. The dashed lines in panels D) and E) show the size distributions produced for mLNPs and mEVs using the "Functionalized Lipid Insertion Method" described in the text. The FAs shown in panel A are an equal mixture of NBD-DSPE and DSPE-PEG2000-maleimide.

Figure 4. Relative miRNA uptake efficiency into HEPG2 cells with different treatments. A) The relative miRNA (i.e., mmu-miR-298-5p) uptake into HepG2 cells under the various treatments: Untreated HepG2 cells (Cells), HepG2 cells treated with DharmaFect 4 transfection reagent and miRNA (Cells + DharmaFect(miRNA)), HepG2 cells treated with EVs and miRNA (Cells + EVs(miRNA)), HepG2 cells treated with mEVs with an $ASGR1_{PAB}$ and containing miRNA (Cells + mEVs($ASGR1_{PAB}$, miRNA), and HepG2 cells treated with mLNPs with an $ASGR1_{PAB}$ and containing miRNA (Cells + mLNPs($ASGR1_{PAB}$, miRNA). The relative miRNA uptake was normalized against the miRNA uptake by DharmaFect(miRNA). The values in the panel represent the mean ± SD of at least three independent experiments. B) Temporal changes in miRNA uptake

efficiency for mLNPs(ASGR1$_{PAB}$, miRNA) (solid squares) and mEVs(ASGR1$_{PAB}$, miRNA) (solid circles) over 72 hours with respect to U6 snRNA. The points and bars represent the average and SD, respectively. The p-values are * $p \leqslant 0.05$, ** $p \leqslant 0.01$, *** $p \leqslant 0.001$, **** $p<0.0001$. Abbreviations: SD, standard deviation.

Figure 5. Anti-proliferative effects miRNA hsa-miR-26a-5p with HepG2 cells under various treatments. A) Microscopic images of a HepG2 layer during the migration assay with the following treatments after 0 (top) and 72 hours (bottom): Untreated HepG2 cells (Cells), HepG2 cells treated with empty EVs (Cells + EVs()), HepG2 cells treated with EVs containing miRNA (EVs(miRNA)), HepG2 cells treated with empty mEVs engineered with an ASGR1$_{PAB}$ (Cells + mEVs(ASGR1$_{PAB}$)), HepG2 cells treated with mEVs with the ASGR1$_{PAB}$ and miRNA (Cells + mEVs(ASGR1$_{PAB}$, miRNA)), and HepG2 cells treated mLNPs with the ASGR1$_{PAB}$ and miRNA (Cells + mLNPs(ASGR1$_{PAB}$, miRNA)). The black bar in the lower left-hand figure represents a distance of 200 μm. B) Shows quantitative measurements of HepG2 cell migration using the data and same abbreviations from panel A. The values in the bar graphs represent the mean ± SD of at least three independent experiments. C) Temporal changes in HepG2 cell migration in untreated cells (open circles) and cells treated with EVs(miRNA) (open squares), mEVs(ASGR1$_{PAB}$, miRNA) (closed circles), and mLNPs(ASGR1$_{PAB}$, miRNA) (closed squares) over 72 hours. To emphasize the differences, the time course for HepG2 cells treated with mEVs(ASGR1$_{PAB}$, miRNA) and mLNPs(ASGR1$_{PAB}$, miRNA) is shown as thick lines. The error bars represent the mean of three independent experiments ± SD. The dose miRNA in each of the experiments was 0.35 μg. The p-values are * $p \leqslant 0.05$, ** $p \leqslant 0.01$, *** $p \leqslant 0.001$, **** $p<0.0001$. Abbreviations: SD, standard deviation.

Figure 6. Process of administering functionalized vesicles into mice. A) On the first day, functionalized vesicles, mEVs or mLNPs, with miRNA (R) and targeting ligands such as Abs are intraperitoneally (IP) injected into mice. B) Three days later, the mice are euthanized, and the organs are harvested. C) RNA is harvested and purified from the mouse organs. D) The amount of purified RNA from each of the organs is analyzed against U6 snRNA by qRT-PCR. E) The relative level of miRNA uptake by the mouse organs from treatment with the functionalized vesicles is determined using the $\Delta\Delta C_t$ method. Abbreviations: R, miRNA.

Figure 7. Uptake of miRNA in organs of mice treated with functionalized vesicles containing the non-targeting polyclonal green fluorescent GFP (GFP_{PAB}) antibodies. The figure shows the relative-fold uptake of miRNA in the organs of mice treated with (A) mEVs(GFP_{PAB}, mmu-miR-298) and (B) mLNPs(GFP_{PAB}, mmu-miR-298) versus mice that were treated with SFM only (black and barely visible in the figure). The data were normalized against the U6 snRNA and expressed as mean ± SEM. The p-values are * $p \leqslant 0.05$, ** $p \leqslant 0.01$, *** $p \leqslant 0.001$, **** $p<0.0001$. Abbreviations: SEM, standard error of the mean.

Figure 8. Targeting of mmu-miR-298 with the ASGR1 antibody in mice. The following figure shows the fold-difference of mmu-miR-298 uptake in various organs of mice after being treated with A) mEVs (n=3) and B) mLNPs (n=6) versus the serum-free media control. The data were normalized to U6 and expressed as mean± SEM of at least three independent samples. The injection volume in the mice varied between 250 and 300 μl. The p-values are * $p \leqslant 0.05$, ** $p \leqslant 0.01$, *** $p \leqslant 0.001$, **** $p<0.0001$. Abbreviations: SEM, standard error of the mean.

Figure 9. Relative mmu-miR-298 uptake by organs with the treatment of mEVs and mLNPs bioengineered with NPHS2 antibody. A) mEVs (n=3) and B) mLNPs (n=6) bioengineered with an NPHS2 antibody in mice. The relative mmu-miR-298 uptake of mice treated with serum-free media (black) and mEVs/mLNPs treated (white). All the data were normalized to the constitutive level of U6 snRNA and represent the mean± SEM. The dosage for each of the mice was approximately 114 μg with an injection volume of 250-300 μl. The p-values are * $p \leqslant 0.05$, ** $p \leqslant 0.01$, *** $p \leqslant 0.001$, **** $p<0.0001$.

Figure 10. ACE2 targeting and immune reactivity of mEV(ACE2) and mLNP(ACE2) in-vivo. The relative ratio of mmu-miR-298 uptake in various organs of mice after being treated with A) mEVs($ACE2_{PAB}$, miRNA) and B) mLNP($ACE2_{PAB}$, miRNA) versus SFM (control) (n=6) in a log scale. The data were normalized to U6 and expressed as mean± SEM of at least three independent experiments. C) Levels of 8-major cytokine factors as obtained after conducting cytokine assay on the blood samples withdrawn from mice treated with mEVs($ACE2_{PAB}$, miRNA) (gray), mLNP($ACE2_{PAB}$, miRNA) (white), and SFM only (black) (n=6) 72 hours after the treatment. The dosage for the mice was 110 μg and the injection volume was 250-300 μl. The p-values are * $p \leqslant 0.05$, ** $p \leqslant 0.01$, *** $p \leqslant 0.001$, **** $p<0.0001$.

1 **Figure 1.**

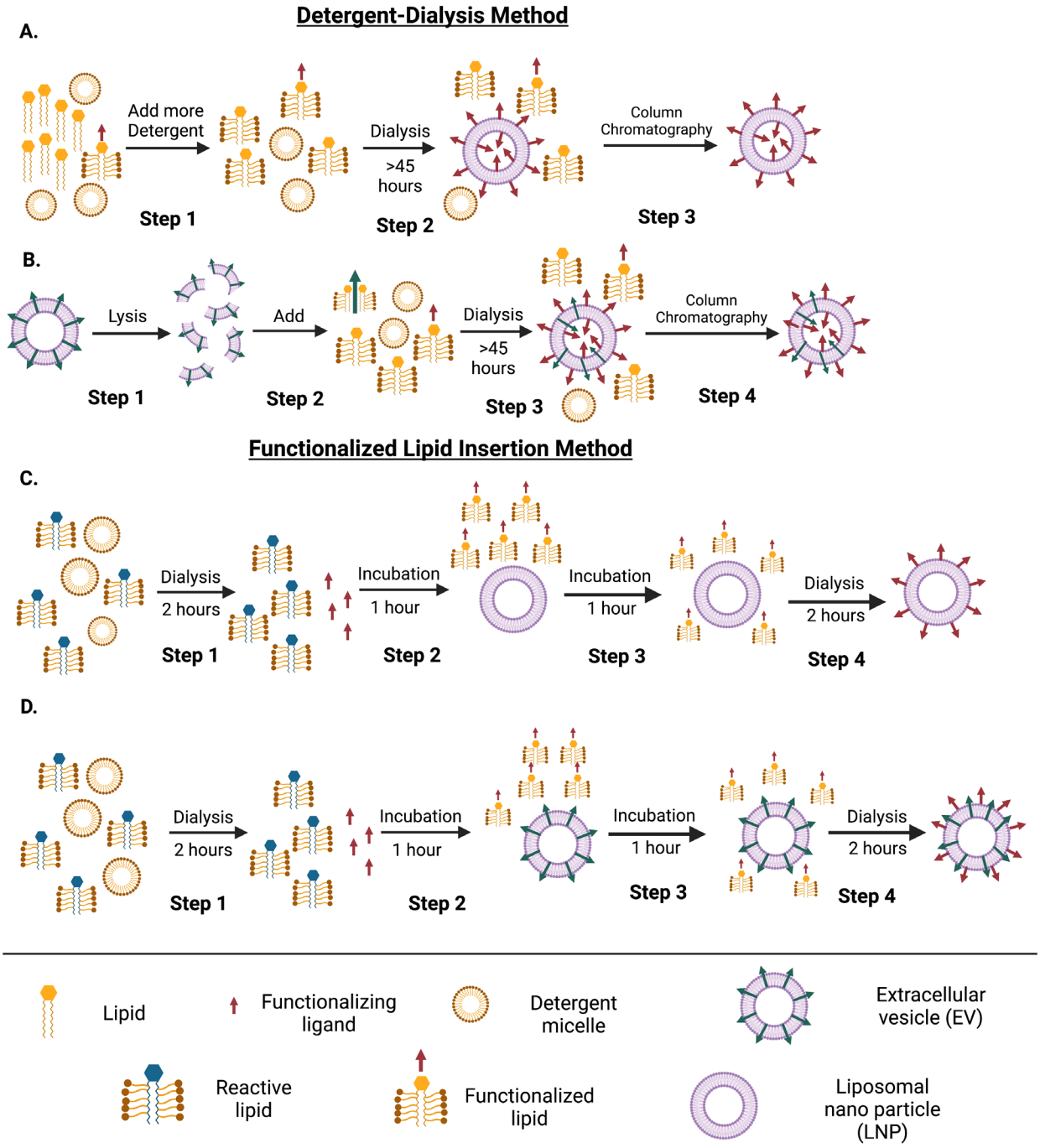

3

4

5

1

2 **Figure 2.**

3

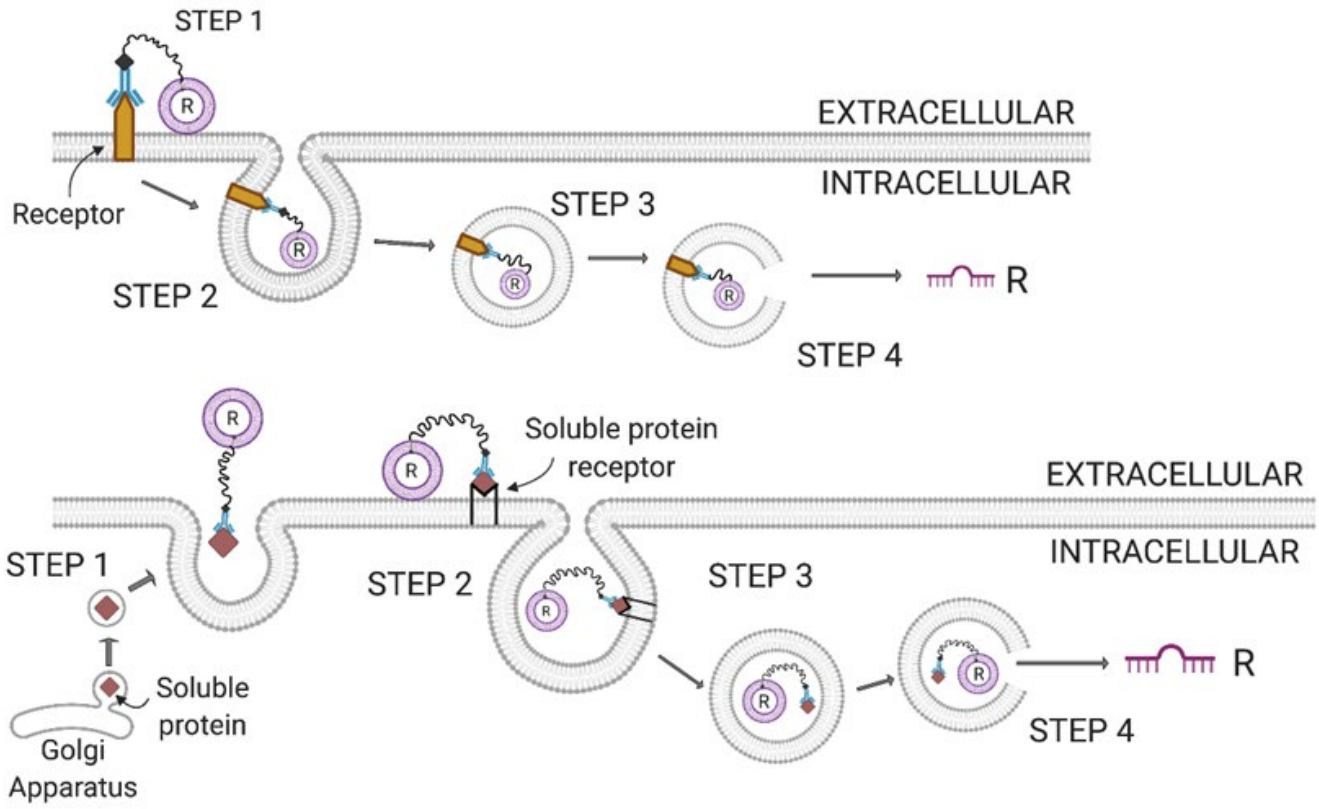
STEP 1
EXTRACELLULAR
INTRACELLULAR
Receptor
STEP 3
STEP 2
R
STEP 4
Soluble protein
receptor
EXTRACELLULAR
INTRACELLULAR
STEP 1
STEP 2
STEP 3
Soluble
protein
Golgi
Apparatus
STEP 4

1 **Figure 3.**

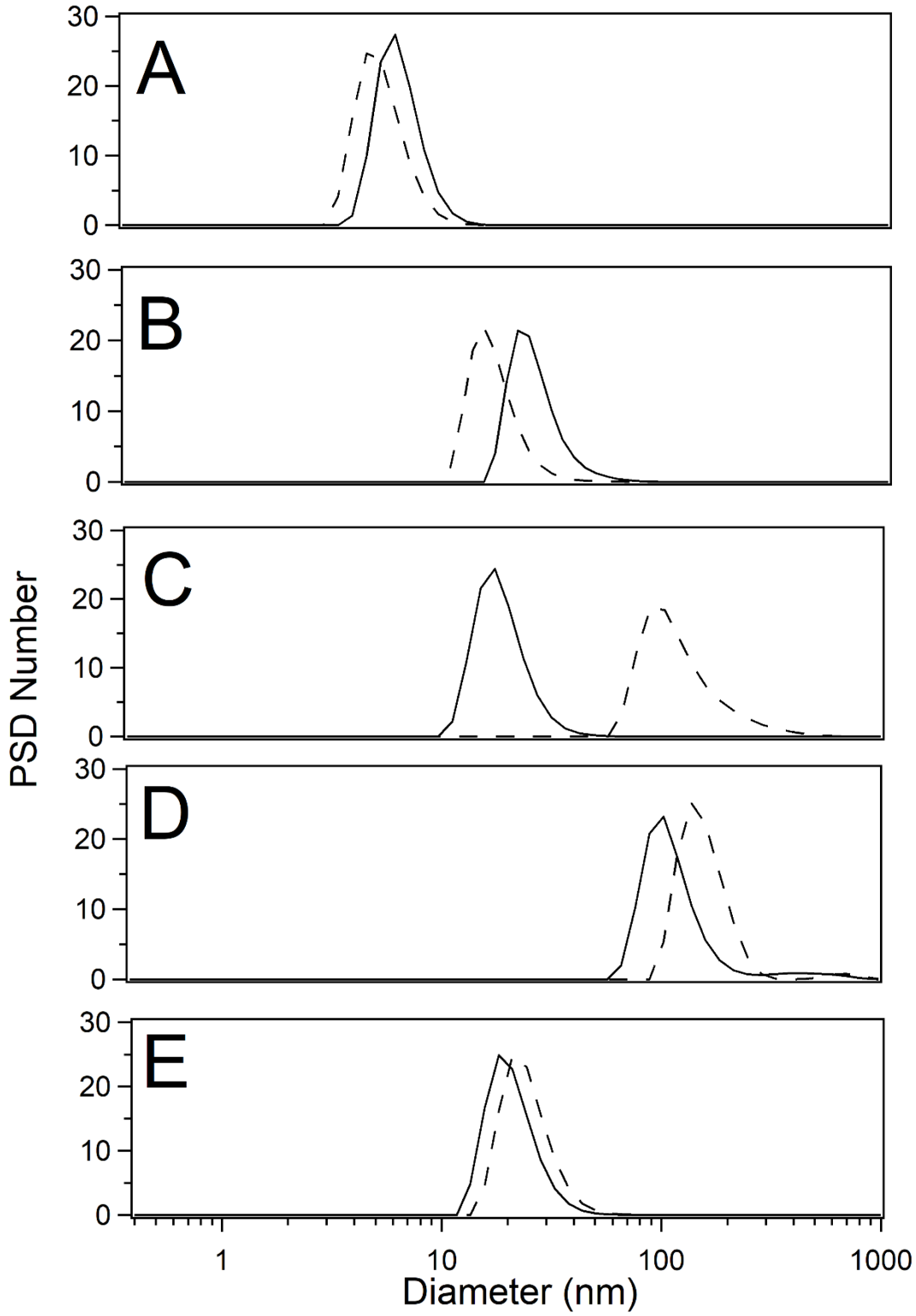

2

3

Figure 4.

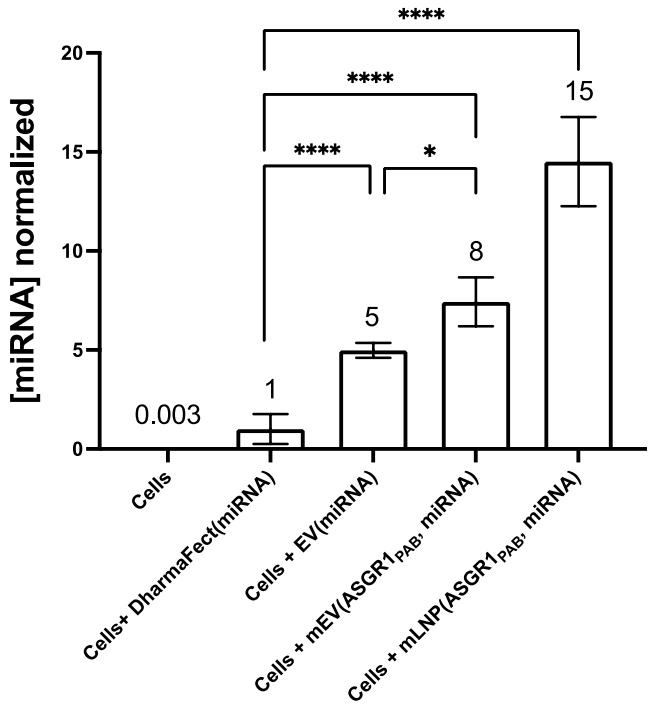
A
[miRNA] normalized
20
15
10
5
0
****
****
****
*
0.003
1
5
8
15
Cells
Cells+ DharmaFect(miRNA)
Cells + EV(miRNA)
Cells + mEV(ASGR1PAB, miRNA)
Cells + mLNP(ASGR1PAB, miRNA)

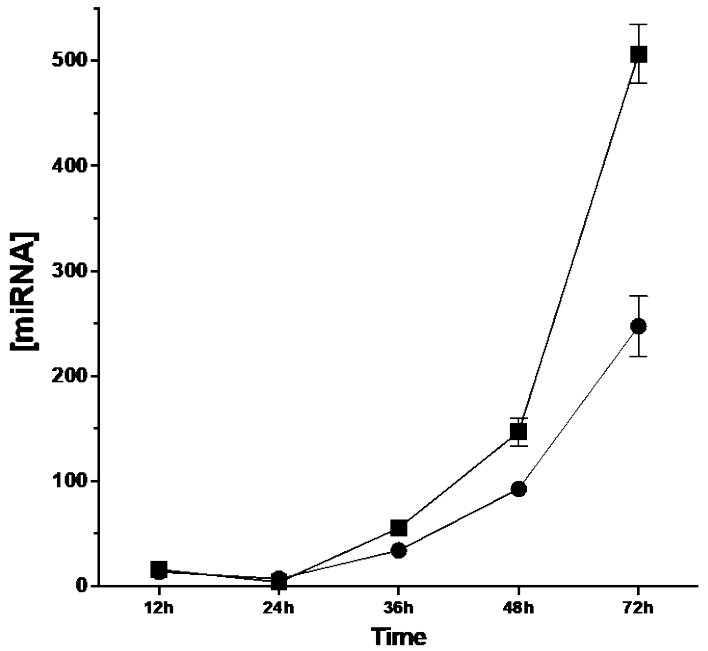
B
[miRNA]
500
400
300
200
100
0
12h
24h
36h
48h
72h
Time

1

2 **Figure 5.**

3

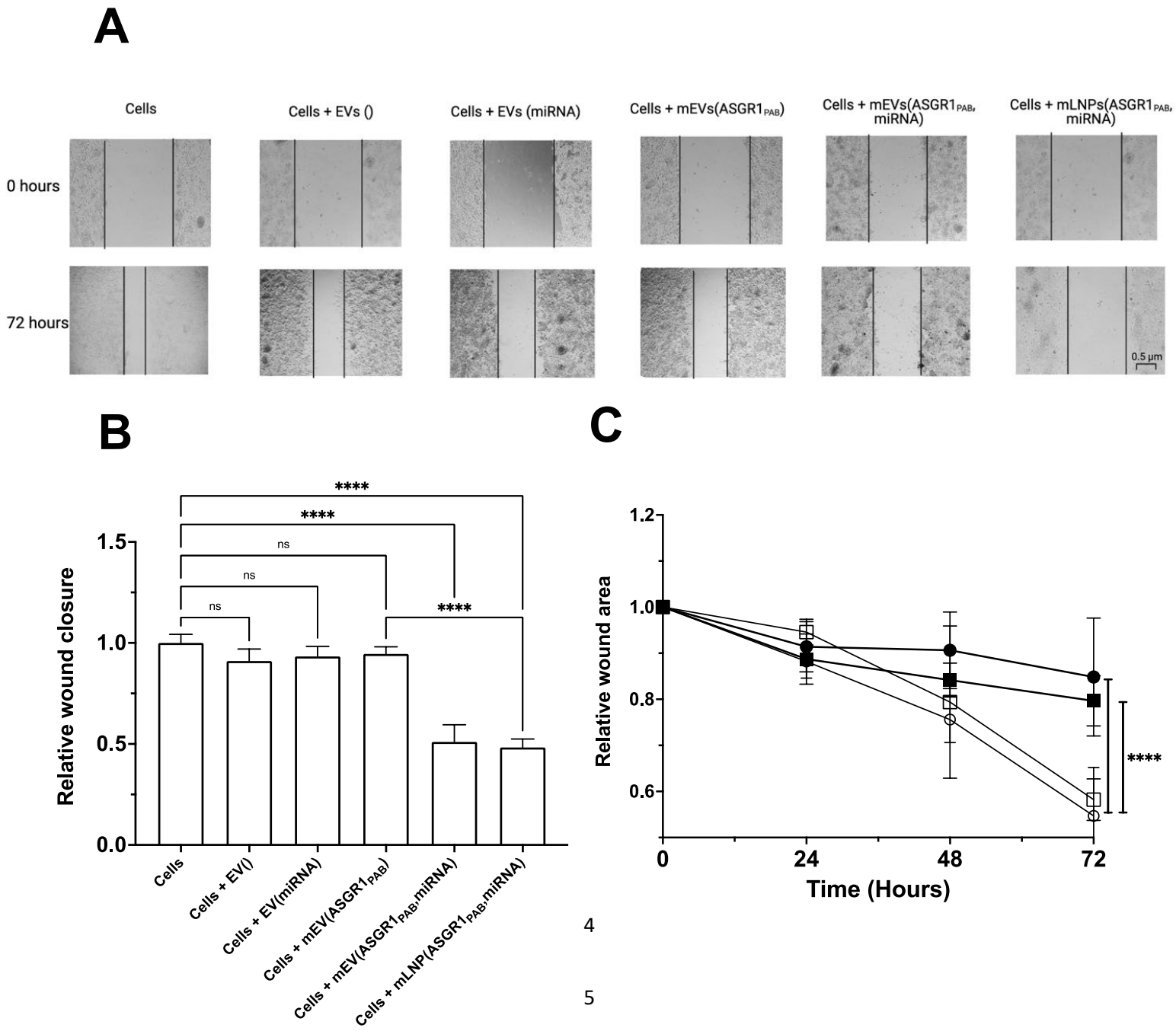

4

5

6

1 **Figure 6.**

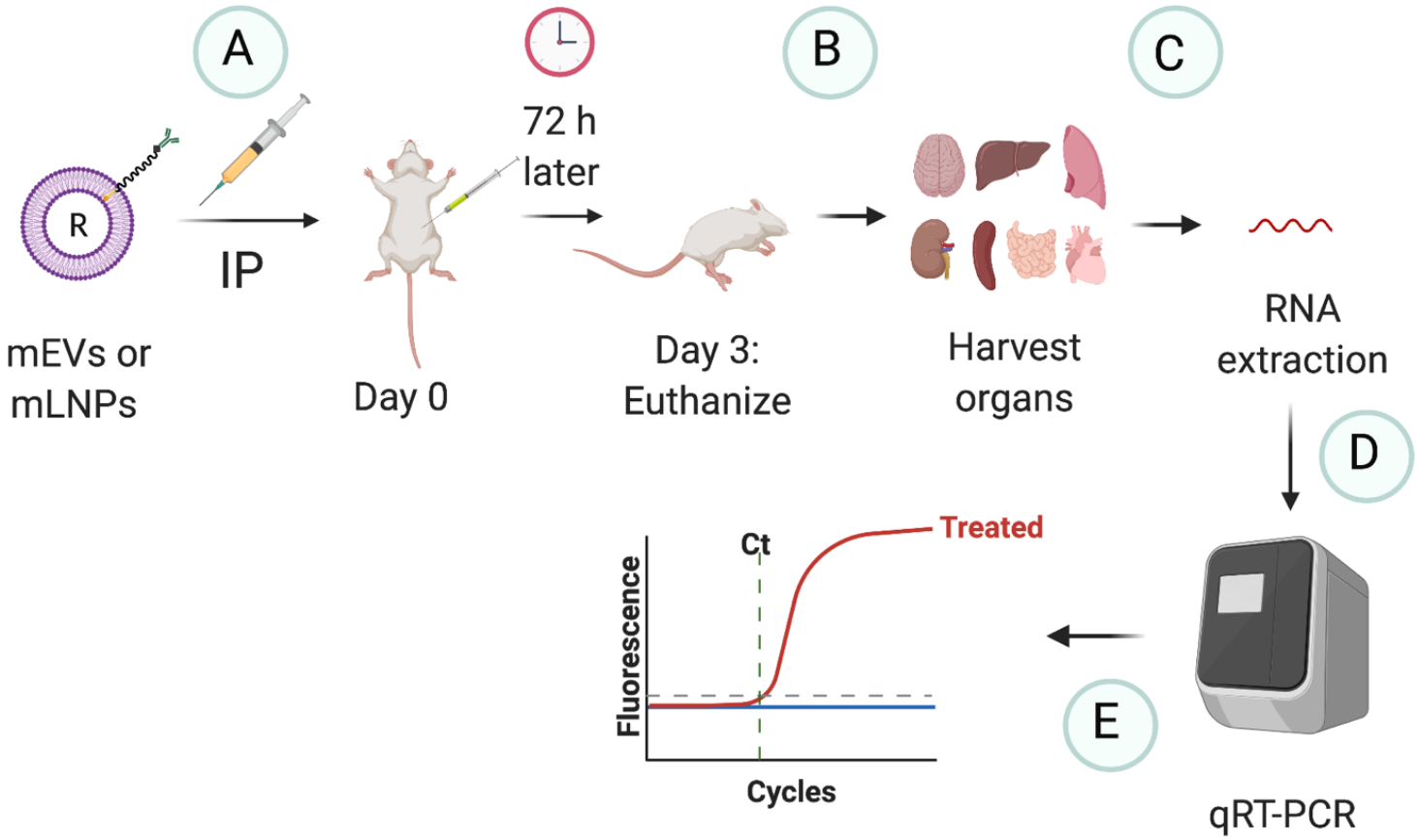
A
B
C
D
E
R
IP
mEVs or
mLNPs
Day 0
72 h
later
Day 3:
Euthanize
Harvest
organs
RNA
extraction
qRT-PCR
Treated
Ct
Fluorescence
Cycles

2

3

Figure 7.

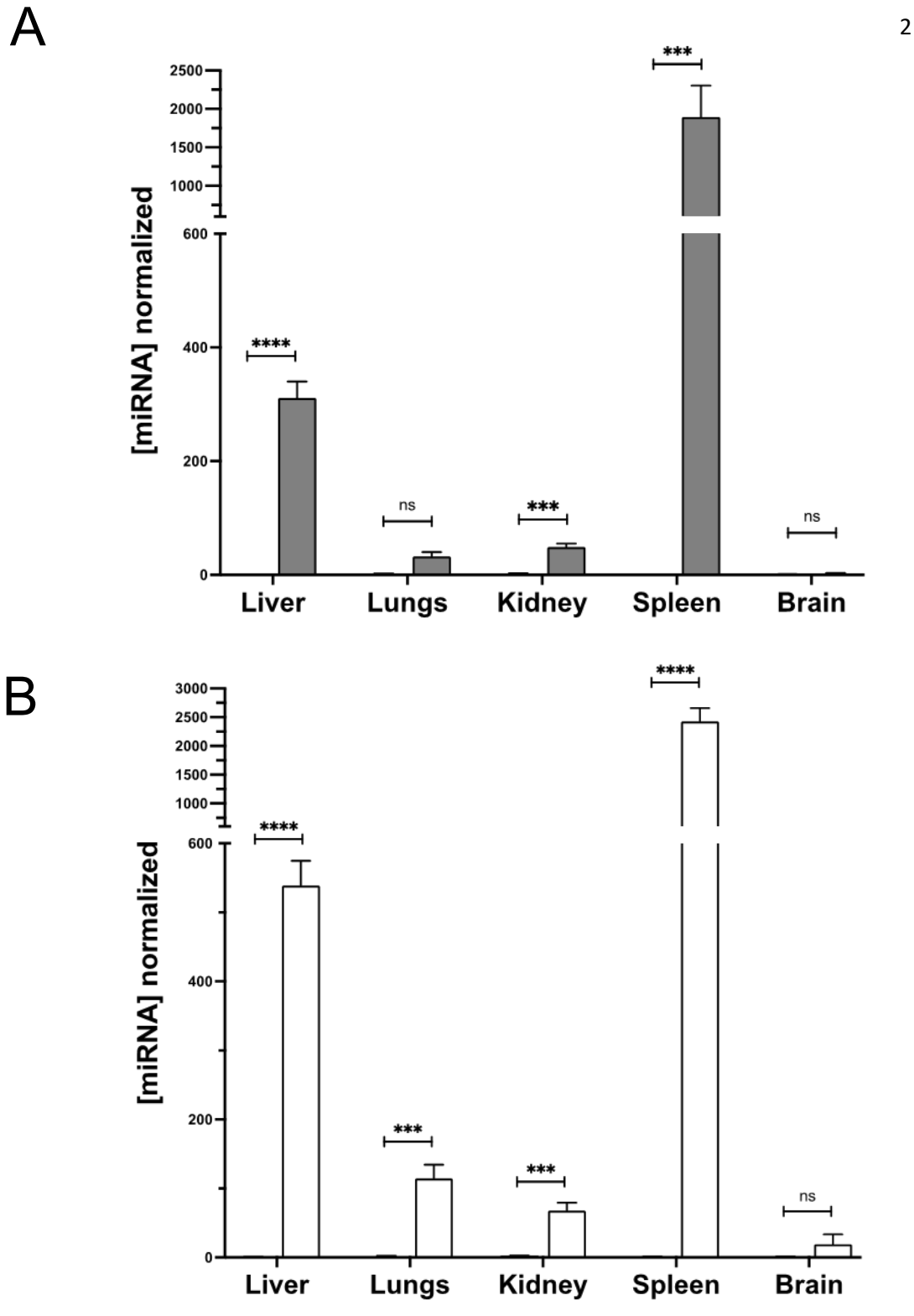
A
[miRNA] normalized
2500
2000
1500
1000
600
400
200
0
****
ns
***
***
ns
Liver
Lungs
Kidney
Spleen
Brain
B
[miRNA] normalized
3000
2500
2000
1500
1000
600
400
200
0
****
***
***
****
ns
Liver
Lungs
Kidney
Spleen
Brain

1 **Figure 8.**

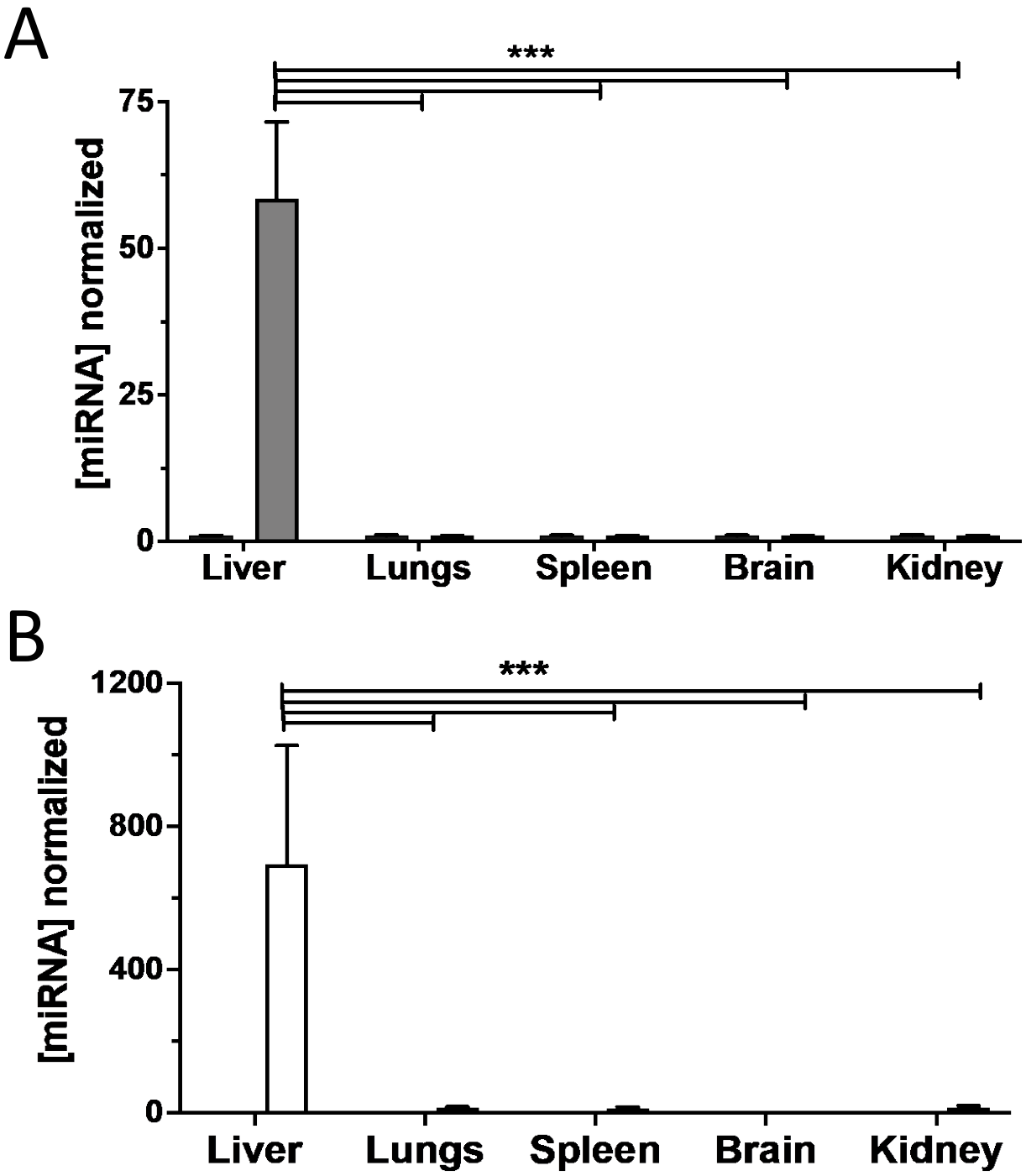
A
***
75
50
25
0
[miRNA] normalized
Liver
Lungs
Spleen
Brain
Kidney
B
***
1200
800
400
0
[miRNA] normalized
Liver
Lungs
Spleen
Brain
Kidney

4

5

Figure 9.

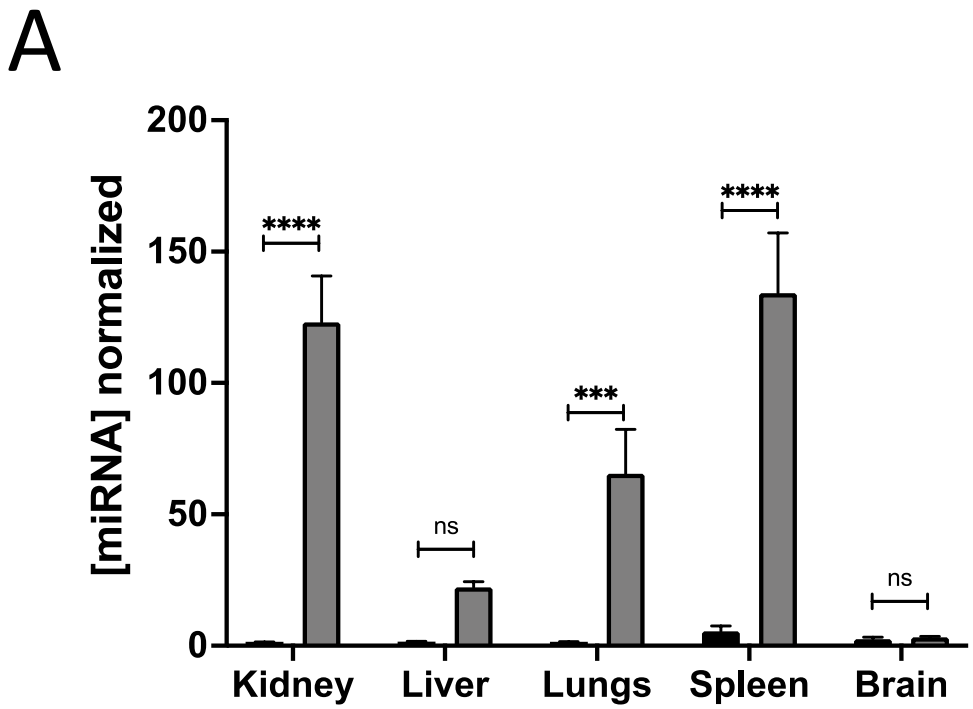
A
[miRNA] normalized
200
150
100
50
0
****
ns
***
****
ns
Kidney
Liver
Lungs
Spleen
Brain

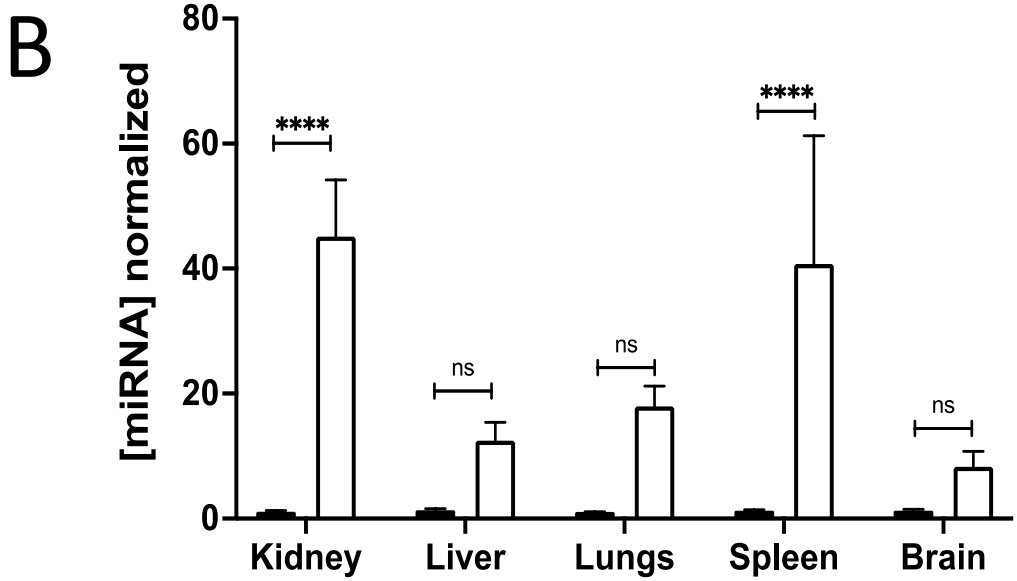
B
[miRNA] normalized
80
60
40
20
0
****
ns
ns
****
ns
Kidney
Liver
Lungs
Spleen
Brain

1 **Figure 10.**

A

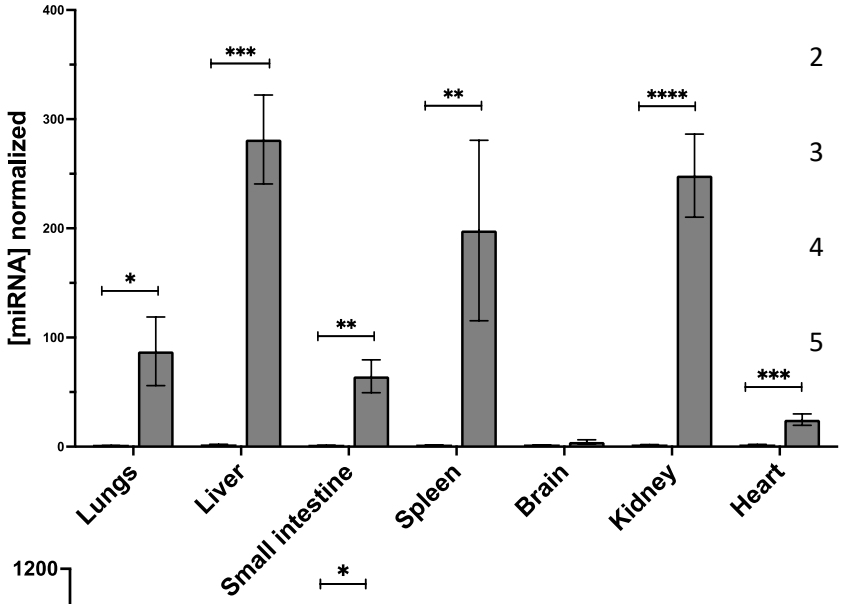

2

3

4

5

B

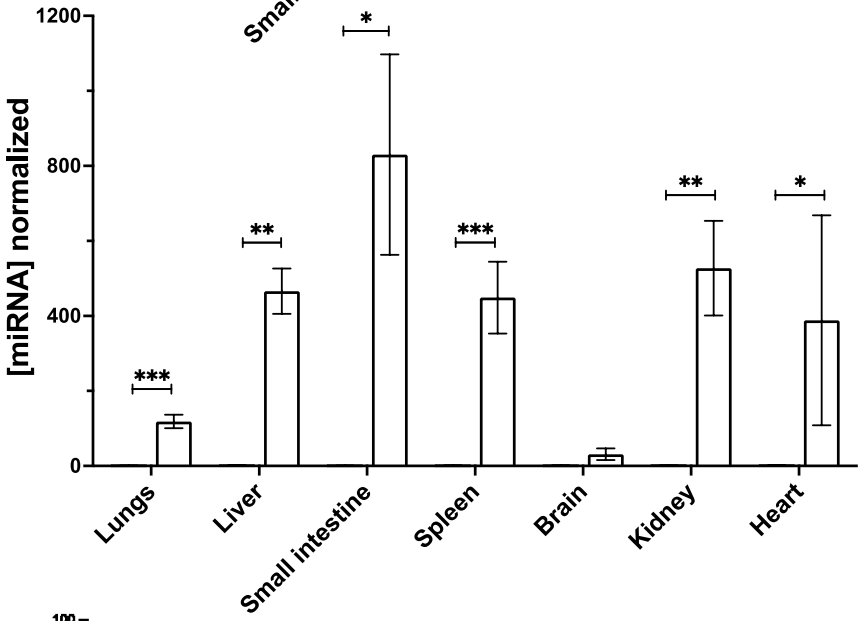

C

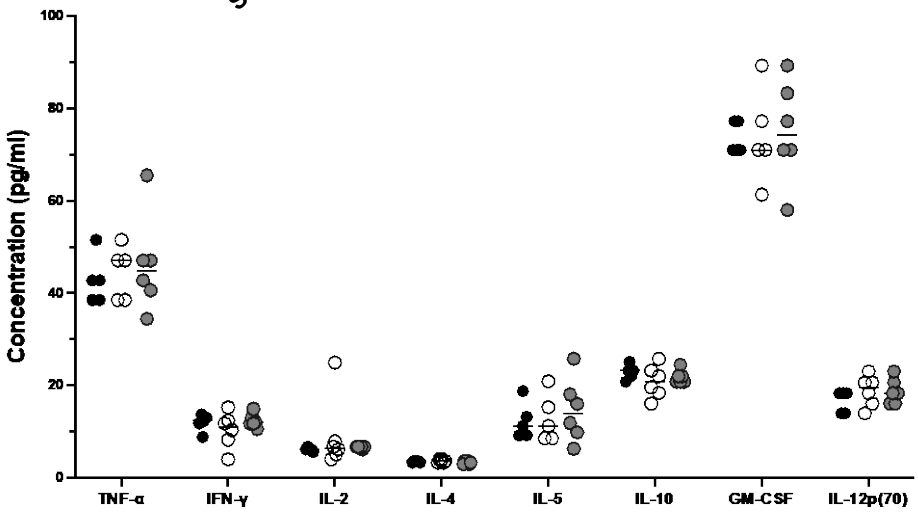

Bibliography

[1] J.K. Patra, G. Das, L.F. Fraceto, E.V.R. Campos, M. del P. Rodriguez-Torres, L.S. Acosta-Torres, L.A. Diaz-Torres, R. Grillo, M.K. Swamy, S. Sharma, S. Habtemariam, H.-S. Shin, Nano based drug delivery systems: recent developments and future prospects, Journal of Nanobiotechnology. 16 (2018) 71. https://doi.org/10.1186/s12951-018-0392-8.

[2] D. Das, N. Maity, A.H. V, Nanotechnology: a revolution in targeted drug delivery, International Journal of Basic & Clinical Pharmacology. 6 (2017) 2766–2773. https://doi.org/10.18203/2319-2003.ijbcp20175200.

[3] B.S. Zolnik, Á. González-Fernández, N. Sadrieh, M.A. Dobrovolskaia, Nanoparticles and the Immune System, Endocrinology. 151 (2010) 458–465. https://doi.org/10.1210/en.2009-1082.

[4] S. Su, P.M. Kang, Systemic Review of Biodegradable Nanomaterials in Nanomedicine, Nanomaterials (Basel). 10 (2020). https://doi.org/10.3390/nano10040656.

[5] X. Li, L. Wang, Y. Fan, Q. Feng, F. Cui, Biocompatibility and Toxicity of Nanoparticles and Nanotubes, Journal of Nanomaterials. 2012 (2012) e548389. https://doi.org/10.1155/2012/548389.

[6] F. Alexis, E. Pridgen, L.K. Molnar, O.C. Farokhzad, Factors Affecting the Clearance and Biodistribution of Polymeric Nanoparticles, Mol Pharm. 5 (2008) 505–515. https://doi.org/10.1021/mp800051m.

[7] S.T. Jahan, S.M.A. Sadat, M. Walliser, A. Haddadi, Targeted Therapeutic Nanoparticles: An Immense Promise to Fight against Cancer, Journal of Drug Delivery. 2017 (2017) e9090325. https://doi.org/10.1155/2017/9090325.

[8] X. Luan, K. Sansanaphongpricha, I. Myers, H. Chen, H. Yuan, D. Sun, Engineering exosomes as refined biological nanoplatforms for drug delivery, Acta Pharmacologica Sinica. 38 (2017) 754–763. https://doi.org/10.1038/aps.2017.12.

[9] A. Akbarzadeh, R. Rezaei-Sadabady, S. Davaran, S.W. Joo, N. Zarghami, Y. Hanifehpour, M. Samiei, M. Kouhi, K. Nejati-Koshki, Liposome: classification, preparation, and applications, Nanoscale Res Lett. 8 (2013) 102. https://doi.org/10.1186/1556-276X-8-102.

[10] E.M. Veziroglu, G.I. Mias, Characterizing Extracellular Vesicles and Their Diverse RNA Contents, Front Genet. 11 (2020) 700. https://doi.org/10.3389/fgene.2020.00700.

[11] R. Kalluri, V.S. LeBleu, The biology, function, and biomedical applications of exosomes, Science. 367 (2020). https://doi.org/10.1126/science.aau6977.

[12] J. Qin, Q. Xu, Functions and application of exosomes, Acta Pol Pharm. 71 (2014) 537–43.

[13] R.R. Sawant, V.P. Torchilin, Challenges in Development of Targeted Liposomal Therapeutics, AAPS J. 14 (2012) 303–315. https://doi.org/10.1208/s12248-012-9330-0.

[14] A. Samad, Y. Sultana, M. Aqil, Liposomal drug delivery systems: an update review, Curr Drug Deliv. 4 (2007) 297–305. https://doi.org/10.2174/156720107782151269.

[15] K. Bryniarski, W. Ptak, A. Jayakumar, K. Püllmann, M.J. Caplan, A. Chairoungdua, J. Lu, B.D. Adams, E. Sikora, K. Nazimek, S. Marquez, S.H. Kleinstein, P. Sangwung, Y. Iwakiri, E. Delgato, F. Redegeld, B.R. Blokhuis, J. Wojcikowski, A.W. Daniel, T.G. Kormelink, P.W. Askenase, Antigen-specific, antibody-coated, exosome-like nanovesicles deliver suppressor T-cell microRNA-150 to effector T cells to inhibit contact sensitivity, Journal of Allergy and Clinical Immunology. 132 (2013) 170-181.e9. https://doi.org/10.1016/j.jaci.2013.04.048.

[16] Y. Si, S. Kim, E. Zhang, Y. Tang, R. Jaskula-Sztul, J.M. Markert, H. Chen, L. Zhou, X. (Margaret) Liu, Targeted Exosomes for Drug Delivery: Biomanufacturing, Surface Tagging, and Validation, Biotechnology Journal. 15 (2020) 1900163. https://doi.org/10.1002/biot.201900163.

[17] A. Huang, L. Huang, S.J. Kennel, Monoclonal antibody covalently coupled with fatty acid. A reagent for in vitro liposome targeting., Journal of Biological Chemistry. 255 (1980) 8015–8018. https://doi.org/10.1016/S0021-9258(19)70595-X.

[18] J.L. Rigaud, D. Levy, Reconstitution of membrane proteins into liposomes, Methods in Enzymology. 372 (2003) 65–86. https://doi.org/10.1016/S0076-6879(03)72004-7.

[19] L.E. Westerman, P.E. Jensen, Liposomes Composed of Reconstituted Membranes for Induction of Tumor-Specific Immunity, in: Methods in Enzymology, Academic Press, 2003: pp. 118–127. https://doi.org/10.1016/S0076-6879(03)73008-0.

[20] A. Huang, S.J. Kennel, L. Huang, Immunoliposome labeling: A sensitive and specific method for cell surface labeling, Journal of Immunological Methods. 46 (1981) 141–151. https://doi.org/10.1016/0022-1759(81)90131-9.

[21] H. Alpes, K. Allmann, H. Plattner, J. Reichert, R. Rick, S. Schulz, Formation of large unilamellar vesicles using alkyl maltoside detergents, Biochimica et Biophysica Acta (BBA) - Biomembranes. 862 (1986) 294–302. https://doi.org/10.1016/0005-2736(86)90231-2.

[22] L. Huang, United States Patent: 4957735 - Target-sensitive immunoliposomes- preparation and characterization, 4957735, 1990. https://patft.uspto.gov/netacgi/nph-Parser?Sect1=PTO1&Sect2=HITOFF&d=PALL&p=1&u=%2Fnetahtml%2FPTO%2Fsrchnum.htm&r=1&f=G&l=50&s1=4,957,735.PN.&OS=PN/4,957,735&RS=PN/4,957,735 (accessed August 31, 2021).

[23] R.J.Y. Ho, B.T. Rouse, L. Huang, Target-sensitive immunoliposomes: preparation and characterization, Biochemistry. 25 (1986) 5500–5506. https://doi.org/10.1021/bi00367a023.

[24] M. Micklus, N. Greig, S. Rapoport, Targeting of liposomes to the blood-brain barrier, US20020025313A1, 2002. https://patents.google.com/patent/US20020025313A1/en (accessed August 21, 2021).

[25] Y. Cheng, Q. Zeng, Q. Han, W. Xia, Effect of pH, temperature and freezing-thawing on quantity changes and cellular uptake of exosomes, Protein Cell. 10 (2019) 295–299. https://doi.org/10.1007/s13238-018-0529-4.

[26] H. Ma, C. Ó'Fágáin, R. O'Kennedy, Antibody stability: A key to performance - Analysis, influences and improvement, Biochimie. 177 (2020) 213–225. https://doi.org/10.1016/j.biochi.2020.08.019.

[27] C.I.E. Smith, R. Zain, Therapeutic Oligonucleotides: State of the Art, Annual Review of Pharmacology and Toxicology. 59 (2019) 605–630. https://doi.org/10.1146/annurev-pharmtox-010818-021050.

[28] T.C. Roberts, R. Langer, M.J.A. Wood, Advances in oligonucleotide drug delivery, Nat Rev Drug Discov. 19 (2020) 673–694. https://doi.org/10.1038/s41573-020-0075-7.

[29] K.E. Lundin, O. Gissberg, C.I.E. Smith, R. Zain, Chemical Development of Therapeutic Oligonucleotides, in: O. Gissberg, R. Zain, K.E. Lundin (Eds.), Oligonucleotide-Based Therapies: Methods and Protocols, Springer, New York, NY, 2019: pp. 3–16. https://doi.org/10.1007/978-1-4939-9670-4_1.

[30] K. Tatiparti, S. Sau, S.K. Kashaw, A.K. Iyer, siRNA Delivery Strategies: A Comprehensive Review of Recent Developments, Nanomaterials. 7 (2017) 77. https://doi.org/10.3390/nano7040077.

[31] K. Gavrilov, W.M. Saltzman, Therapeutic siRNA: Principles, Challenges, and Strategies, Yale J Biol Med. 85 (2012) 187–200.

[32] K. Dhuri, C. Bechtold, E. Quijano, H. Pham, A. Gupta, A. Vikram, R. Bahal, Antisense Oligonucleotides: An Emerging Area in Drug Discovery and Development, Journal of Clinical Medicine. 9 (2020) 2004. https://doi.org/10.3390/jcm9062004.

[33] M. Gagliardi, A.T. Ashizawa, The Challenges and Strategies of Antisense Oligonucleotide Drug Delivery, Biomedicines. 9 (2021) 433. https://doi.org/10.3390/biomedicines9040433.

[34] R. Rupaimoole, F.J. Slack, MicroRNA therapeutics: towards a new era for the management of cancer and other diseases, Nat Rev Drug Discov. 16 (2017) 203–222. https://doi.org/10.1038/nrd.2016.246.

[35] R.C. Wilson, J.A. Doudna, Molecular Mechanisms of RNA Interference, Annual Review of Biophysics. 42 (2013) 217–239. https://doi.org/10.1146/annurev-biophys-083012-130404.

[36] M.M. Zhang, R. Bahal, T.P. Rasmussen, J.E. Manautou, X. Zhong, The growth of siRNA-based therapeutics: Updated clinical studies, Biochemical Pharmacology. 189 (2021) 114432. https://doi.org/10.1016/j.bcp.2021.114432.

[37] S. Akhtar, M.D. Hughes, A. Khan, M. Bibby, M. Hussain, Q. Nawaz, J. Double, P. Sayyed, The delivery of antisense therapeutics, Advanced Drug Delivery Reviews. 44 (2000) 3–21. https://doi.org/10.1016/S0169-409X(00)00080-6.

[38] J. O'Brien, H. Hayder, Y. Zayed, C. Peng, Overview of MicroRNA Biogenesis, Mechanisms of Actions, and Circulation, Front. Endocrinol. 9 (2018). https://doi.org/10.3389/fendo.2018.00402.

[39] C.E. Condrat, D.C. Thompson, M.G. Barbu, O.L. Bugnar, A. Boboc, D. Cretoiu, N. Suciu, S.M. Cretoiu, S.C. Voinea, miRNAs as Biomarkers in Disease: Latest Findings Regarding Their Role in Diagnosis and Prognosis, Cells. 9 (2020). https://doi.org/10.3390/cells9020276.

[40] W. Si, J. Shen, H. Zheng, W. Fan, The role and mechanisms of action of microRNAs in cancer drug resistance, Clinical Epigenetics. 11 (2019) 25. https://doi.org/10.1186/s13148-018-0587-8.

[41] A. Jeyaram, S.M. Jay, Preservation and Storage Stability of Extracellular Vesicles for Therapeutic Applications, AAPS J. 20 (2017) 1. https://doi.org/10.1208/s12248-017-0160-y.

[42] S.K. Panda, B. Ravindran, F. Histopaque, Isolation of human PBMCs, Bio-Protocol. 3 (2013) e323.

[43] G.E. Moore, R.E. Gerner, H.A. Franklin, Culture of Normal Human Leukocytes, JAMA. 199 (1967) 519–524. https://doi.org/10.1001/jama.1967.03120080053007.

[44] B. Mui, L. Chow, M.J. Hope, Extrusion technique to generate liposomes of defined size, Methods in Enzymology. 367 (2003) 3–14. https://doi.org/10.1016/S0076-6879(03)67001-1.

[45] K.V. Ledwitch, R.W. Barnes, A.G. Roberts, Unravelling the complex drug-drug interactions of the cardiovascular drugs, verapamil and digoxin, with P-glycoprotein, Biosci. Rep. 36 (2016) 1–14. https://doi.org/10.1042/BSR20150317.

[46] J.P. Kampf, D. Cupp, A.M. Kleinfeld, Different Mechanisms of Free Fatty Acid Flip-Flop and Dissociation Revealed by Temperature and Molecular Species Dependence of Transport across Lipid Vesicles*, Journal of Biological Chemistry. 281 (2006) 21566–21574. https://doi.org/10.1074/jbc.M602067200.

[47] S. Hupfeld, A.M. Holsæter, M. Skar, C.B. Frantzen, M. Brandl, Liposome Size Analysis by Dynamic/Static Light Scattering upon Size Exclusion-/Field Flow-Fractionation, Journal of Nanoscience and Nanotechnology. 6 (2006) 3025–3031. https://doi.org/10.1166/jnn.2006.454.

[48] G. Liang, S. Kan, Y. Zhu, S. Feng, W. Feng, S. Gao, Engineered exosome-mediated delivery of functionally active miR-26a and its enhanced suppression effect in HepG2 cells, Int J Nanomedicine. 13 (2018) 585–599. https://doi.org/10.2147/IJN.S154458.

[49] O. López, A. de la Maza, L. Coderch, C. López-Iglesias, E. Wehrli, J.L. Parra, Direct formation of mixed micelles in the solubilization of phospholipid liposomes by Triton X-100, FEBS Letters. 426 (1998) 314–318. https://doi.org/10.1016/S0014-5793(98)00363-9.

[50] V. Palmieri, D. Lucchetti, I. Gatto, A. Maiorana, M. Marcantoni, G. Maulucci, M. Papi, R. Pola, M. De Spirito, A. Sgambato, Dynamic light scattering for the characterization and counting of extracellular vesicles: a powerful noninvasive tool, J Nanopart Res. 16 (2014) 2583. https://doi.org/10.1007/s11051-014-2583-z.

[51] R. Szatanek, M. Baj-Krzyworzeka, J. Zimoch, M. Lekka, M. Siedlar, J. Baran, The Methods of Choice for Extracellular Vesicles (EVs) Characterization, Int J Mol Sci. 18 (2017). https://doi.org/10.3390/ijms18061153.

[52] I. Makra, P. Terejánszky, R.E. Gyurcsányi, A method based on light scattering to estimate the concentration of virus particles without the need for virus particle standards, MethodsX. 2 (2015) 91–99. https://doi.org/10.1016/j.mex.2015.02.003.

[53] L. Alvarez-Erviti, Y. Seow, H. Yin, C. Betts, S. Lakhal, M.J.A. Wood, Delivery of siRNA to the mouse brain by systemic injection of targeted exosomes, Nature Biotechnology. 29 (2011) 341–345. https://doi.org/10.1038/nbt.1807.

[54] S. Pirkmajer, A.V. Chibalin, Serum starvation: caveat emptor, American Journal of Physiology-Cell Physiology. 301 (2011) C272–C279. https://doi.org/10.1152/ajpcell.00091.2011.

[55] M.W. Pfaffl, Relative quantitation, in: M.T. Dorak (Ed.), Real-Time PCR, 1st edition, Taylor & Francis, 2007.

[56] A.L. Didychuk, S.E. Butcher, D.A. Brow, The life of U6 small nuclear RNA, from cradle to grave, RNA. 24 (2018) 437–460. https://doi.org/10.1261/rna.065136.117.

[57] R.L. Causin, D. Pessôa-Pereira, K.C.B. Souza, A.F. Evangelista, R.M.V. Reis, J.H.T.G. Fregnani, M.M.C. Marques, Identification and performance evaluation of housekeeping genes for microRNA expression normalization by reverse transcription-quantitative PCR using liquid-based cervical cytology samples, Oncol Lett. 18 (2019) 4753–4761. https://doi.org/10.3892/ol.2019.10824.

[58] T.D. Schmittgen, K.J. Livak, Analyzing real-time PCR data by the comparative C T method, Nature Protocols. 3 (2008) 1101–1108. https://doi.org/10.1038/nprot.2008.73.

[59] I. Hamming, M. Cooper, B. Haagmans, N. Hooper, R. Korstanje, A. Osterhaus, W. Timens, A. Turner, G. Navis, H. van Goor, The emerging role of ACE2 in physiology and disease, J Pathol. 212 (2007) 1–11. https://doi.org/10.1002/path.2162.

[60] I. Hamming, W. Timens, M. Bulthuis, A. Lely, G. Navis, H. van Goor, Tissue distribution of ACE2 protein, the functional receptor for SARS coronavirus. A first step in understanding SARS pathogenesis, J Pathol. 203 (2004) 631–637. https://doi.org/10.1002/path.1570.

[61] C. Km, S. Ml, R. An, K. La, Carbon Dioxide for Euthanasia: Concerns Regarding Pain and Distress, With Special Reference to Mice and Rats, Laboratory Animals. 39 (2005). https://doi.org/10.1258/0023677053739747.

[62] TRIzol Products - US, (n.d.). https://www.thermofisher.com/us/en/home/brands/product-brand/trizol.html (accessed May 16, 2020).

[63] Bio-Plex Pro™ Mouse Cytokine, Chemokine, and Growth Factor Assays | Life Science Research | Bio-Rad, (n.d.). https://www.bio-rad.com/en-us/category/bio-plex-pro-mouse-cytokine-chemokine-growth-factor-assays?ID=37dd4c58-2aa7-4991-a7cb-5c51024959c6 (accessed December 11, 2020).

[64] L.A. Mulcahy, R.C. Pink, D.R.F. Carter, Routes and mechanisms of extracellular vesicle uptake, J Extracell Vesicles. 3 (2014). https://doi.org/10.3402/jev.v3.24641.

[65] G. Costaguta, G.S. Payne, Overview of Protein Trafficking Mechanisms, in: N. Segev (Ed.), Trafficking Inside Cells: Pathways, Mechanisms and Regulation, Springer, New York, NY, 2009: pp. 105–118. https://doi.org/10.1007/978-0-387-93877-6_6.

[66] A. Perrakis, W.H. Moolenaar, Autotaxin: structure-function and signaling, J. Lipid Res. 55 (2014) 1010–1018. https://doi.org/10.1194/jlr.R046391.

[67] J. Stetefeld, S.A. McKenna, T.R. Patel, Dynamic light scattering: a practical guide and applications in biomedical sciences, Biophys Rev. 8 (2016) 409–427. https://doi.org/10.1007/s12551-016-0218-6.

[68] P.M. Carvalho, M.R. Felício, N.C. Santos, S. Gonçalves, M.M. Domingues, Application of Light Scattering Techniques to Nanoparticle Characterization and Development, Frontiers in Chemistry. 6 (2018) 237. https://doi.org/10.3389/fchem.2018.00237.

[69] K.L. Linegar, A.E. Adeniran, A.F. Kostko, M.A. Anisimov, Hydrodynamic radius of polyethylene glycol in solution obtained by dynamic light scattering, Colloid J. 72 (2010) 279–281. https://doi.org/10.1134/S1061933X10020195.

[70] S. Niimi, [Determination of the particle size and relative light scattering intensity of aggregates of human IgG and humanized monoclonal antibody product induced by various stress using dynamic light scattering], Kokuritsu Iyakuhin Shokuhin Eisei Kenkyusho Hokoku. (2011) 55–60.

[71] S. Hu, L. Musante, D. Tataruch, X. Xu, O. Kretz, M. Henry, P. Meleady, H. Luo, H. Zou, Y. Jiang, H. Holthofer, Purification and Identification of Membrane Proteins from Urinary Extracellular Vesicles using Triton X-114 Phase Partitioning, J. Proteome Res. 17 (2018) 86–96. https://doi.org/10.1021/acs.jproteome.7b00386.

[72] M.T. Donato, L. Tolosa, M.J. Gómez-Lechón, Culture and Functional Characterization of Human Hepatoma HepG2 Cells, Methods Mol. Biol. 1250 (2015) 77–93. https://doi.org/10.1007/978-1-4939-2074-7_5.

[73] S. Wilkening, F. Stahl, A. Bader, Comparison of Primary Human Hepatocytes and Hepatoma Cell Line Hepg2 with Regard to Their Biotransformation Properties, Drug Metab Dispos. 31 (2003) 1035–1042. https://doi.org/10.1124/dmd.31.8.1035.

[74] G.-H. Qiu, X. Xie, F. Xu, X. Shi, Y. Wang, L. Deng, Distinctive pharmacological differences between liver cancer cell lines HepG2 and Hep3B, Cytotechnology. 67 (2015) 1–12. https://doi.org/10.1007/s10616-014-9761-9.

[75] D. Witzigmann, L. Quagliata, S.H. Schenk, C. Quintavalle, L.M. Terracciano, J. Huwyler, Variable asialoglycoprotein receptor 1 expression in liver disease: Implications for therapeutic intervention, Hepatology Research. 46 (2016) 686–696. https://doi.org/10.1111/hepr.12599.

[76] S. Das, P. Kudale, P. Dandekar, P.V. Devarajan, Asialoglycoprotein Receptor and Targeting Strategies, in: P.V. Devarajan, P. Dandekar, A.A. D'Souza (Eds.), Targeted

Intracellular Drug Delivery by Receptor Mediated Endocytosis, Springer International Publishing, Cham, 2019: pp. 353–381. https://doi.org/10.1007/978-3-030-29168-6_12.

[77] Z. Shen, W. Wei, H. Tanaka, K. Kohama, G. Ma, T. Dobashi, Y. Maki, H. Wang, J. Bi, S. Dai, A galactosamine-mediated drug delivery carrier for targeted liver cancer therapy, Pharmacological Research. 64 (2011) 410–419. https://doi.org/10.1016/j.phrs.2011.06.015.

[78] S. Pranatharthiharan, M.D. Patel, V.C. Malshe, V. Pujari, A. Gorakshakar, M. Madkaikar, K. Ghosh, P.V. Devarajan, Asialoglycoprotein receptor targeted delivery of doxorubicin nanoparticles for hepatocellular carcinoma, Drug Delivery. 24 (2017) 20–29. https://doi.org/10.1080/10717544.2016.1225856.

[79] M. Wei, Y. Xu, Q. Zou, L. Tu, C. Tang, T. Xu, L. Deng, C. Wu, Hepatocellular carcinoma targeting effect of PEGylated liposomes modified with lactoferrin, European Journal of Pharmaceutical Sciences. 46 (2012) 131–141. https://doi.org/10.1016/j.ejps.2012.02.007.

[80] A.A. D'Souza, P.V. Devarajan, Asialoglycoprotein receptor mediated hepatocyte targeting — Strategies and applications, Journal of Controlled Release. 203 (2015) 126–139. https://doi.org/10.1016/j.jconrel.2015.02.022.

[81] L. Bao, S. Hazari, S. Mehra, D. Kaushal, K. Moroz, S. Dash, Increased expression of P-glycoprotein and doxorubicin chemoresistance of metastatic breast cancer is regulated by miR-298, Am. J. Pathol. 180 (2012) 2490–2503. https://doi.org/10.1016/j.ajpath.2012.02.024.

[82] Y. Xie, Y. Shao, X. Deng, M. Wang, Y. Chen, MicroRNA-298 Reverses Multidrug Resistance to Antiepileptic Drugs by Suppressing MDR1/P-gp Expression in vitro, Front Neurosci. 12 (2018). https://doi.org/10.3389/fnins.2018.00602.

[83] A. Kozomara, M. Birgaoanu, S. Griffiths-Jones, miRBase: from microRNA sequences to function, Nucleic Acids Res. 47 (2019) D155–D162. https://doi.org/10.1093/nar/gky1141.

[84] P.E. Marques, S. Nyegaard, R.F. Collins, F. Troise, S.A. Freeman, W.S. Trimble, S. Grinstein, Multimerization and Retention of the Scavenger Receptor SR-B1 in the Plasma Membrane, Developmental Cell. 50 (2019) 283-295.e5. https://doi.org/10.1016/j.devcel.2019.05.026.

[85] D. Sahoo, Y.F. Darlington, D. Pop, D.L. Williams, M.A. Connelly, Scavenger receptor class B Type I (SR-BI) assembles into detergent-sensitive dimers and tetramers, Biochimica et Biophysica Acta (BBA) - Molecular and Cell Biology of Lipids. 1771 (2007) 807–817. https://doi.org/10.1016/j.bbalip.2006.03.003.

[86] X. Cui, K. Song, X. Lu, W. Feng, W. Di, Liposomal Delivery of MicroRNA-7 Targeting EGFR to Inhibit the Growth, Invasion, and Migration of Ovarian Cancer, ACS Omega. (2021). https://doi.org/10.1021/acsomega.1c00992.

[87] M.T.D. Martino, V. Campani, G. Misso, M.E.G. Cantafio, A. Gullà, U. Foresta, P.H. Guzzi, M. Castellano, A. Grimaldi, V. Gigantino, R. Franco, S. Lusa, M. Cannataro, P. Tagliaferri, G.D. Rosa, P. Tassone, M. Caraglia, In Vivo Activity of MiR-34a Mimics Delivered by Stable Nucleic Acid Lipid Particles (SNALPs) against Multiple Myeloma, PLOS ONE. 9 (2014) e90005. https://doi.org/10.1371/journal.pone.0090005.

[88] A. Stamm, K. Reimers, S. Strauß, P. Vogt, T. Scheper, I. Pepelanova, In vitro wound healing assays – state of the art, BioNanoMaterials. 17 (2016) 79–87. https://doi.org/10.1515/bnm-2016-0002.

[89] J.E.N. Jonkman, J.A. Cathcart, F. Xu, M.E. Bartolini, J.E. Amon, K.M. Stevens, P. Colarusso, An introduction to the wound healing assay using live-cell microscopy, Cell Adhesion & Migration. 8 (2014) 440–451. https://doi.org/10.4161/cam.36224.

[90] M.J. Haney, Y. Zhao, J. Fay, H. Duhyeong, M. Wang, H. Wang, Z. Li, Y.Z. Lee, M.K. Karuppan, N. El-Hage, A.V. Kabanov, E.V. Batrakova, Genetically modified macrophages accomplish targeted gene delivery to the inflamed brain in transgenic Parkin Q311X(A)

mice: importance of administration routes, Scientific Reports. 10 (2020) 11818. https://doi.org/10.1038/s41598-020-68874-7.

[91] O.P.B. Wiklander, J.Z. Nordin, A. O'Loughlin, Y. Gustafsson, G. Corso, I. Mäger, P. Vader, Y. Lee, H. Sork, Y. Seow, N. Heldring, L. Alvarez-Erviti, C.E. Smith, K. Le Blanc, P. Macchiarini, P. Jungebluth, M.J.A. Wood, S.E. Andaloussi, Extracellular vesicle in vivo biodistribution is determined by cell source, route of administration and targeting, J Extracell Vesicles. 4 (2015) 10.3402/jev.v4.26316. https://doi.org/10.3402/jev.v4.26316.

[92] P. Rosa, F. Clementi, Absorption and Tissue Distribution of Doxorubicin Entrapped in Liposomes following Intravenous or Intraperitoneal Administration, PHA. 26 (1983) 221–229. https://doi.org/10.1159/000137805.

[93] G. Lee, S. Han, I. Inocencio, E. Cao, J. Hong, A.R.J. Phillips, J.A. Windsor, C.J.H. Porter, N.L. Trevaskis, Lymphatic Uptake of Liposomes after Intraperitoneal Administration Primarily Occurs via the Diaphragmatic Lymphatics and is Dependent on Liposome Surface Properties, Mol. Pharmaceutics. 16 (2019) 4987–4999. https://doi.org/10.1021/acs.molpharmaceut.9b00855.

[94] Z. Xueying, L. Zhelong, S. Wenqi, Y. Guodong, X. Changyang, Y. Lijun, Delivery Efficacy Differences of Intravenous and Intraperitoneal Injection of Exosomes: Perspectives from Tracking Dye Labeled and MiRNA Encapsulated Exosomes, Current Drug Delivery. 17 (2020) 186–194.

[95] H. Sun, D. Zhong, C. Wang, Y. Sun, J. Zhao, G. Li, MiR-298 Exacerbates Ischemia/Reperfusion Injury Following Ischemic Stroke by Targeting Act1, CPB. 48 (2018) 528–539. https://doi.org/10.1159/000491810.

[96] V. Boissonneault, I. Plante, S. Rivest, P. Provost, MicroRNA-298 and MicroRNA-328 Regulate Expression of Mouse β-Amyloid Precursor Protein-converting Enzyme 1 *, Journal of Biological Chemistry. 284 (2009) 1971–1981. https://doi.org/10.1074/jbc.M807530200.

[97] D. Barbagallo, S. Piro, A.G. Condorelli, L.G. Mascali, F. Urbano, N. Parrinello, A. Monello, L. Statello, M. Ragusa, A.M. Rabuazzo, C. Di Pietro, F. Purrello, M. Purrello, miR-296-3p, miR-298-5p and their downstream networks are causally involved in the higher resistance of mammalian pancreatic α cells to cytokine-induced apoptosis as compared to β cells, BMC Genomics. 14 (2013) 62. https://doi.org/10.1186/1471-2164-14-62.

[98] N. Bushati, S.M. Cohen, microRNA Functions, Annual Review of Cell and Developmental Biology. 23 (2007) 175–205. https://doi.org/10.1146/annurev.cellbio.23.090506.123406.

[99] X. Li, M. Commane, H. Nie, X. Hua, M. Chatterjee-Kishore, D. Wald, M. Haag, G.R. Stark, Act1, an NF-κB-activating protein, PNAS. 97 (2000) 10489–10493. https://doi.org/10.1073/pnas.160265197.

[100] V. Agarwal, G.W. Bell, J.-W. Nam, D.P. Bartel, Predicting effective microRNA target sites in mammalian mRNAs, ELife. 4 (2015) e05005. https://doi.org/10.7554/eLife.05005.

[101] Y. Chen, X. Wang, miRDB: an online database for prediction of functional microRNA targets, Nucleic Acids Research. 48 (2020) D127–D131. https://doi.org/10.1093/nar/gkz757.

[102] L.-L. Kong, X.-M. Zhuang, H.-Y. Yang, M. Yuan, L. Xu, H. Li, Inhibition of P-glycoprotein Gene Expression and Function Enhances Triptolide-induced Hepatotoxicity in Mice, Sci Rep. 5 (2015) 11747. https://doi.org/10.1038/srep11747.

[103] E.A. Greenfield, ed., Antibodies A Laboratory Manual, Second edition, Illustrated edition, Cold Spring Harbor Laboratory Press, Cold Spring Harbor, New York, 2013.

[104] H. Kim, N.C. Berens, N.E. Ochandarena, B.D. Philpot, Region and Cell Type Distribution of TCF4 in the Postnatal Mouse Brain, Frontiers in Neuroanatomy. 14 (2020) 42. https://doi.org/10.3389/fnana.2020.00042.

[105] M. Dell'Aringa, R.L. Reinhardt, Notch signaling represents an important checkpoint between follicular T-helper and canonical T-helper 2 cell fate, Mucosal Immunol. 11 (2018) 1079–1091. https://doi.org/10.1038/s41385-018-0012-9.

[106] R.E. Mebius, G. Kraal, Structure and function of the spleen, Nat Rev Immunol. 5 (2005) 606–616. https://doi.org/10.1038/nri1669.

[107] L.A. Medina, R. Klipper, W.T. Phillips, B. Goins, Pharmacokinetics and biodistribution of [111In]-avidin and [99mTc]-biotin-liposomes injected in the pleural space for the targeting of mediastinal nodes, Nuclear Medicine and Biology. 31 (2004) 41–51. https://doi.org/10.1016/S0969-8051(03)00122-7.

[108] K. Schwarz, M. Simons, J. Reiser, M.A. Saleem, C. Faul, W. Kriz, A.S. Shaw, L.B. Holzman, P. Mundel, Podocin, a raft-associated component of the glomerular slit diaphragm, interacts with CD2AP and nephrin, J Clin Invest. 108 (2001) 1621–1629. https://doi.org/10.1172/JCI12849.

[109] Polyclonal vs. monoclonal antibodies, (n.d.). https://www.ptglab.com/news/blog/polyclonal-vs-monoclonal-antibodies/ (accessed July 30, 2021).

[110] What is a polyclonal antibody? - Ximbio FAQ, (n.d.). https://ximbio.com/faq/57/what-is-a-polyclonal-antibody (accessed July 30, 2021).

[111] P. Towler, B. Staker, S.G. Prasad, S. Menon, J. Tang, T. Parsons, D. Ryan, M. Fisher, D. Williams, N.A. Dales, M.A. Patane, M.W. Pantoliano, ACE2 X-Ray Structures Reveal a Large Hinge-bending Motion Important for Inhibitor Binding and Catalysis*, Journal of Biological Chemistry. 279 (2004) 17996–18007. https://doi.org/10.1074/jbc.M311191200.

[112] A.J. Turner, Chapter 25 - ACE2 Cell Biology, Regulation, and Physiological Functions, in: T. Unger, U.M. Steckelings, R.A.S. dos Santos (Eds.), The Protective Arm of the Renin Angiotensin System (RAS), Academic Press, Boston, 2015: pp. 185–189. https://doi.org/10.1016/B978-0-12-801364-9.00025-0.

[113] M. Donoghue, F. Hsieh, E. Baronas, K. Godbout, M. Gosselin, N. Stagliano, M. Donovan, B. Woolf, K. Robison, R. Jeyaseelan, R.E. Breitbart, S. Acton, A novel angiotensin-converting enzyme-related carboxypeptidase (ACE2) converts angiotensin I to angiotensin 1-9, Circ Res. 87 (2000) E1-9. https://doi.org/10.1161/01.res.87.5.e1.

[114] D. Harmer, M. Gilbert, R. Borman, K.L. Clark, Quantitative mRNA expression profiling of ACE 2, a novel homologue of angiotensin converting enzyme, FEBS Letters. 532 (2002) 107–110. https://doi.org/10.1016/S0014-5793(02)03640-2.

[115] F. Gembardt, A. Sterner-Kock, H. Imboden, M. Spalteholz, F. Reibitz, H.-P. Schultheiss, W.-E. Siems, T. Walther, Organ-specific distribution of ACE2 mRNA and correlating peptidase activity in rodents, Peptides. 26 (2005) 1270–1277. https://doi.org/10.1016/j.peptides.2005.01.009.

[116] S. Romagnani, T-cell subsets (Th1 versus Th2), Annals of Allergy, Asthma & Immunology. 85 (2000) 21. https://doi.org/10.1016/S1081-1206(10)62426-X.

[117] S. Kodidela, S. Ranjit, N. Sinha, C. McArthur, A. Kumar, S. Kumar, Cytokine profiling of exosomes derived from the plasma of HIV-infected alcohol drinkers and cigarette smokers, PLOS ONE. 13 (2018) e0201144. https://doi.org/10.1371/journal.pone.0201144.

[118] M.T. Abrams, M.L. Koser, J. Seitzer, S.C. Williams, M.A. DiPietro, W. Wang, A.W. Shaw, X. Mao, V. Jadhav, J.P. Davide, P.A. Burke, A.B. Sachs, S.M. Stirdivant, L. Sepp-Lorenzino, Evaluation of Efficacy, Biodistribution, and Inflammation for a Potent siRNA Nanoparticle: Effect of Dexamethasone Co-treatment, Molecular Therapy. 18 (2010) 171–180. https://doi.org/10.1038/mt.2009.208.

[119] Q. Pan, V. Ramakrishnaiah, S. Henry, S. Fouraschen, P.E. de Ruiter, J. Kwekkeboom, H.W. Tilanus, H.L.A. Janssen, L.J.W. van der Laan, Hepatic cell-to-cell transmission of small silencing RNA can extend the therapeutic reach of RNA interference (RNAi), Gut. 61 (2012) 1330–1339. https://doi.org/10.1136/gutjnl-2011-300449.

[120] H. Nie, X. Xie, D. Zhang, Y. Zhou, B. Li, F. Li, F. Li, Y. Cheng, H. Mei, H. Meng, L. Jia, Use of lung-specific exosomes for miRNA-126 delivery in non-small cell lung cancer, Nanoscale. 12 (2020) 877–887. https://doi.org/10.1039/C9NR09011H.

[121] C. Liu, C. Su, Design strategies and application progress of therapeutic exosomes, Theranostics. 9 (2019) 1015–1028. https://doi.org/10.7150/thno.30853.

[122] G. Liang, Y. Zhu, D.J. Ali, T. Tian, H. Xu, K. Si, B. Sun, B. Chen, Z. Xiao, Engineered exosomes for targeted co-delivery of miR-21 inhibitor and chemotherapeutics to reverse drug resistance in colon cancer, Journal of Nanobiotechnology. 18 (2020) 10. https://doi.org/10.1186/s12951-019-0563-2.

[123] C. Meyer, J. Losacco, Z. Stickney, L. Li, G. Marriott, B. Lu, Pseudotyping exosomes for enhanced protein delivery in mammalian cells, IJN. 12 (2017) 3153–3170. https://doi.org/10.2147/IJN.S133430.

[124] S. Hsu, B. Yu, X. Wang, Y. Lu, C.R. Schmidt, R.J. Lee, L.J. Lee, S.T. Jacob, K. Ghoshal, Cationic lipid nanoparticles for therapeutic delivery of siRNA and miRNA to murine liver tumor, Nanomedicine: Nanotechnology, Biology and Medicine. 9 (2013) 1169–1180. https://doi.org/10.1016/j.nano.2013.05.007.

[125] Y. Akao, Y. Nakagawa, I. Hirata, A. Iio, T. Itoh, K. Kojima, R. Nakashima, Y. Kitade, T. Naoe, Role of anti-oncomirs miR-143 and -145 in human colorectal tumors, Cancer Gene Ther. 17 (2010) 398–408. https://doi.org/10.1038/cgt.2009.88.

[126] Y. Wu, M. Crawford, B. Yu, Y. Mao, S.P. Nana-Sinkam, L.J. Lee, MicroRNA Delivery by Cationic Lipoplexes for Lung Cancer Therapy, Mol. Pharmaceutics. 8 (2011) 1381–1389. https://doi.org/10.1021/mp2002076.

[127] Y. Wu, M. Crawford, Y. Mao, R.J. Lee, I.C. Davis, T.S. Elton, L.J. Lee, S.P. Nana-Sinkam, Therapeutic Delivery of MicroRNA-29b by Cationic Lipoplexes for Lung Cancer, Molecular Therapy - Nucleic Acids. 2 (2013) e84. https://doi.org/10.1038/mtna.2013.14.

[128] L. Jiang, H. Wang, S. Chen, Aptamer (AS1411)-Conjugated Liposome for Enhanced Therapeutic Efficacy of miRNA-29b in Ovarian Cancer, Journal of Nanoscience and Nanotechnology. 20 (2020) 2025–2031.

[129] Y. Chen, X. Zhu, X. Zhang, B. Liu, L. Huang, Nanoparticles Modified With Tumor-targeting scFv Deliver siRNA and miRNA for Cancer Therapy, Molecular Therapy. 18 (2010) 1650–1656. https://doi.org/10.1038/mt.2010.136.

[130] L. Wang, T.-T. Liang, CD59 receptor targeted delivery of miRNA-1284 and cisplatin-loaded liposomes for effective therapeutic efficacy against cervical cancer cells, AMB Express. 10 (2020) 1–11.

[131] D.L. Iden, T.M. Allen, In vitro and in vivo comparison of immunoliposomes made by conventional coupling techniques with those made by a new post-insertion approach, Biochimica et Biophysica Acta (BBA) - Biomembranes. 1513 (2001) 207–216. https://doi.org/10.1016/S0005-2736(01)00357-1.

[132] C. Guo, Y. Chen, W. Gao, A. Chang, Y. Ye, W. Shen, Y. Luo, S. Yang, P. Sun, R. Xiang, N. Li, Liposomal Nanoparticles Carrying anti-IL6R Antibody to the Tumour Microenvironment Inhibit Metastasis in Two Molecular Subtypes of Breast Cancer Mouse Models, Theranostics. 7 (2017) 775–788. https://doi.org/10.7150/thno.17237.

[133] Optimization of post-insertion method to conjugate Doxil with anti-CD133 monoclonal antibodies: Investigating the specific binding and cytotoxicity to colorectal cancer cells in vitro - ScienceDirect, (n.d.). https://www.sciencedirect.com/science/article/pii/S1319016420302097 (accessed September 14, 2021).

[134] R.W. Baker, B.T. Low, Membrane Separation☆, in: Reference Module in Chemistry, Molecular Sciences and Chemical Engineering, Elsevier, 2015. https://doi.org/10.1016/B978-0-12-409547-2.11674-9.

[135] M. Sack, J. Sigler, S. Frenzel, Chr. Eing, J. Arnold, Th. Michelberger, W. Frey, F. Attmann, L. Stukenbrock, G. Müller, Research on Industrial-Scale Electroporation Devices Fostering the Extraction of Substances from Biological Tissue, Food Eng. Rev. 2 (2010) 147–156. https://doi.org/10.1007/s12393-010-9017-1.

[136] S. Kosuri, G.M. Church, Large-scale de novo DNA synthesis: technologies and applications, Nature Methods. 11 (2014) 499–507. https://doi.org/10.1038/nmeth.2918.

[137] J.F. Buyel, R.M. Twyman, R. Fischer, Very-Large-Scale Production of Monoclonal Antibodies in Plants, in: Process Scale Purification of Antibodies, John Wiley & Sons, Ltd, 2017: pp. 655–672. https://doi.org/10.1002/9781119126942.ch30.

[138] A.T. Reiner, K.W. Witwer, B.W.M. van Balkom, J. de Beer, C. Brodie, R.L. Corteling, S. Gabrielsson, M. Gimona, A.G. Ibrahim, D. de Kleijn, C.P. Lai, J. Lötvall, H.A. del Portillo, I.G. Reischl, M. Riazifar, C. Salomon, H. Tahara, W.S. Toh, M.H.M. Wauben, V.K. Yang, Y. Yang, R.W.Y. Yeo, H. Yin, B. Giebel, E. Rohde, S.K. Lim, Concise Review: Developing Best-Practice Models for the Therapeutic Use of Extracellular Vesicles, STEM CELLS Translational Medicine. 6 (2017) 1730–1739. https://doi.org/10.1002/sctm.17-0055.

[139] B. Adriano, N.M. Cotto, N. Chauhan, M. Jaggi, S.C. Chauhan, M.M. Yallapu, Milk exosomes: Nature's abundant nanoplatform for theranostic applications, Bioactive Materials. 6 (2021) 2479–2490. https://doi.org/10.1016/j.bioactmat.2021.01.009.

[140] B. Yu, R.J. Lee, L.J. Lee, Chapter 7 - Microfluidic Methods for Production of Liposomes, in: Methods in Enzymology, Academic Press, 2009: pp. 129–141. https://doi.org/10.1016/S0076-6879(09)65007-2.

[141] C. Walsh, K. Ou, N.M. Belliveau, T.J. Leaver, A.W. Wild, J. Huft, P.J. Lin, S. Chen, A.K. Leung, J.B. Lee, C.L. Hansen, R.J. Taylor, E.C. Ramsay, P.R. Cullis, Microfluidic-based manufacture of siRNA-lipid nanoparticles for therapeutic applications, Methods Mol Biol. 1141 (2014) 109–120. https://doi.org/10.1007/978-1-4939-0363-4_6.

[142] C. Charoenviriyakul, Y. Takahashi, M. Nishikawa, Y. Takakura, Preservation of exosomes at room temperature using lyophilization, International Journal of Pharmaceutics. 553 (2018) 1–7. https://doi.org/10.1016/j.ijpharm.2018.10.032.

[143] P.J. Stevens, R.J. Lee, Formulation kit for liposomal doxorubicin composed of lyophilized liposomes, Anticancer Res. 23 (2003) 439–442.

[144] Full article: Preparation and Characterization of Lyophilized Liposomes with Incorporated Quercetin, (n.d.).

https://www.tandfonline.com/doi/full/10.1080/08982100500528594?casa_token=1GdStm2RxIIAAAAA%3AVRdurySrx65ftzPPDjrEC5mVUU6lETpUTD7hKIYp__fJkuuunElVUblXKlm8mxS-fJG_pvQMo3RDF2g (accessed September 14, 2021).

[145] M. Glavas-Dodov, E. Fredro-Kumbaradzi, K. Goracinova, M. Simonoska, S. Calis, S. Trajkovic-Jolevska, A.A. Hincal, The effects of lyophilization on the stability of liposomes containing 5-FU, International Journal of Pharmaceutics. 291 (2005) 79–86. https://doi.org/10.1016/j.ijpharm.2004.07.045.

[146] T. Hernández-Caselles, J. Villalaín, J.C. Gómez-Fernández, Stability of Liposomes on Long Term Storage, Journal of Pharmacy and Pharmacology. 42 (1990) 397–400. https://doi.org/10.1111/j.2042-7158.1990.tb06578.x.

[147] P.R. Matias-Garcia, R. Wilson, V. Mussack, E. Reischl, M. Waldenberger, C. Gieger, G. Anton, A. Peters, A. Kuehn-Steven, Impact of long-term storage and freeze-thawing on eight circulating microRNAs in plasma samples, PLOS ONE. 15 (2020) e0227648. https://doi.org/10.1371/journal.pone.0227648.

[148] E.W. R., W. H., N. Y., C. J., Improving the Stability of Aptamers by Chemical Modification, Current Medicinal Chemistry. 18 (2011) 4126–4138.

[149] Q. Ge, Y. Zhou, J. Lu, Y. Bai, X. Xie, Z. Lu, miRNA in Plasma Exosome is Stable under Different Storage Conditions, Molecules. 19 (2014) 1568–1575. https://doi.org/10.3390/molecules19021568.

[150] ICMJE | Recommendations | Defining the Role of Authors and Contributors, (n.d.). http://www.icmje.org/recommendations/browse/roles-and-responsibilities/defining-the-role-of-authors-and-contributors.html (accessed July 29, 2020).

[151] D.B. Resnik, A.M. Tyle, J.R. Black, G. Kissling, Authorship policies of scientific journals, J Med Ethics. 42 (2016) 199–202. https://doi.org/10.1136/medethics-2015-103171.

[152] E.E. Tarkang, M. Kweku, F.B. Zotor, Publication Practices and Responsible Authorship: A Review Article, J Public Health Afr. 8 (2017). https://doi.org/10.4081/jphia.2017.723.

[153]K. Strange, Authorship: why not just toss a coin?, Am J Physiol Cell Physiol. 295 (2008) C567–C575. https://doi.org/10.1152/ajpcell.00208.2008.

Figure 1

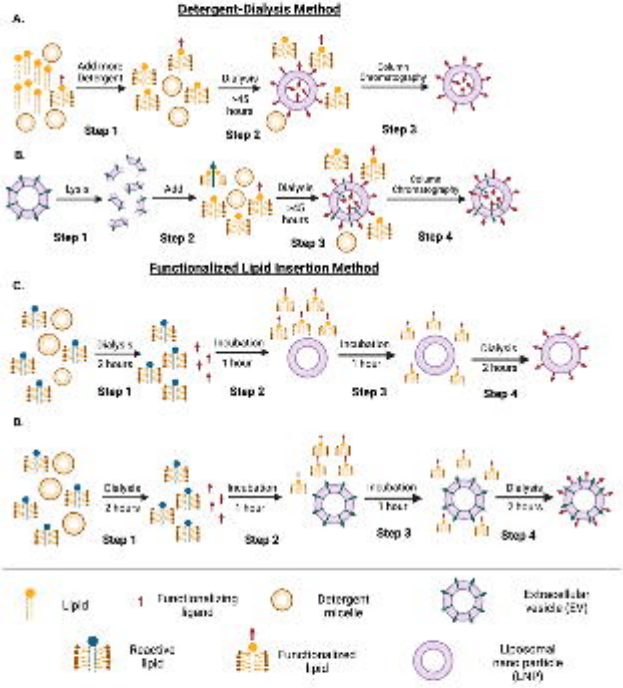
Detergent-Dialysis Method
A.
Add more detergent
Dialysis >48 hours
Column chromatography
Step 1
Step 2
Step 3
B.
Lyse
Add
Dialysis >48 hours
Column chromatography
Step 1
Step 2
Step 3
Step 4
Functionalized Lipid Insertion Method
C.
Dialysis 2 hours
Incubation 1 hour
Incubation 1 hour
Dialysis 2 hours
Step 1
Step 2
Step 3
Step 4
D.
Dialysis 2 hours
Incubation 1 hour
Incubation 1 hour
Dialysis 2 hours
Step 1
Step 2
Step 3
Step 4
Lipid
Functionalizing ligand
Detergent micelle
Extracellular vesicle (EV)
Reactive lipid
Functionalized lipid
Liposomal nanoparticle (LNP)

Figure 2

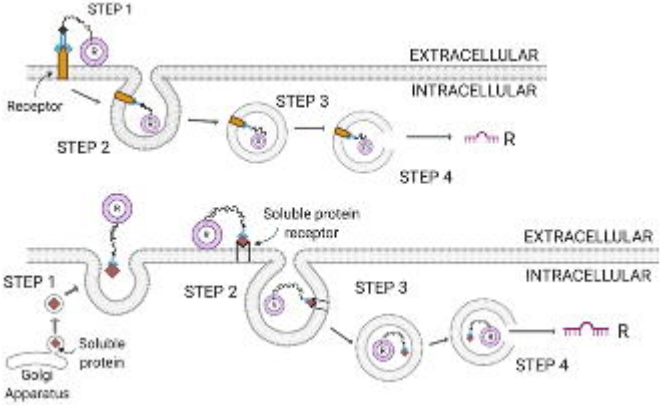
STEP 1
EXTRACELLULAR
INTRACELLULAR
Receptor
STEP 3
STEP 2
R
STEP 4
Soluble protein
receptor
EXTRACELLULAR
STEP 1
INTRACELLULAR
STEP 2
STEP 3
R
Soluble
protein
Golgi
Apparatus
STEP 4

Figure 3

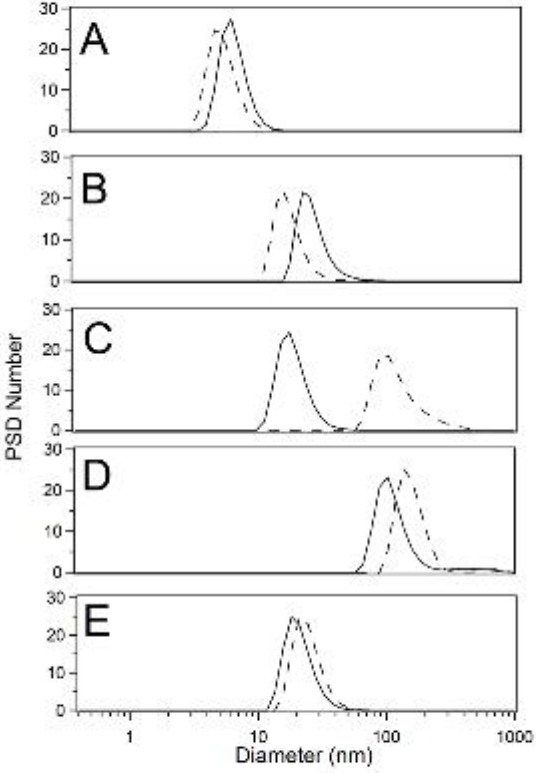

Figure 4

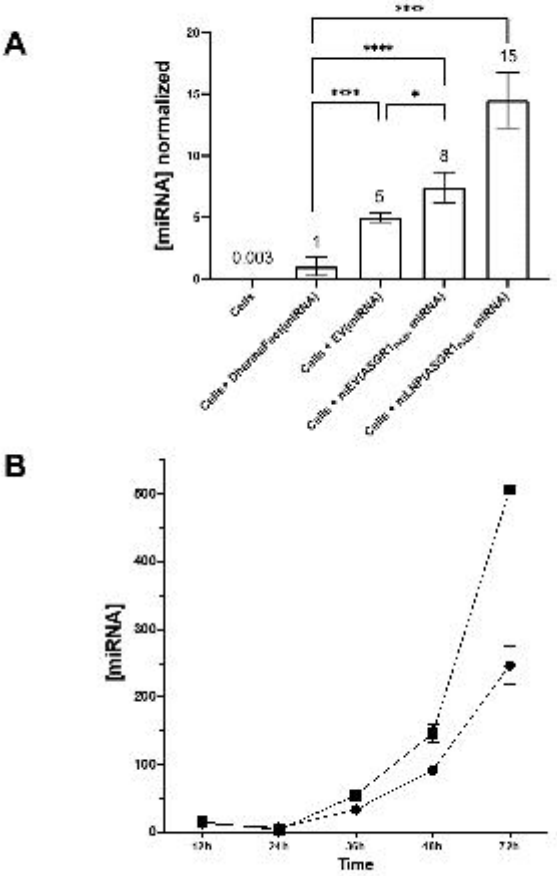

Figure 5

A

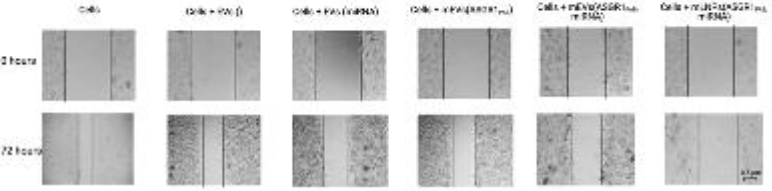
0 hours
72 hours

B

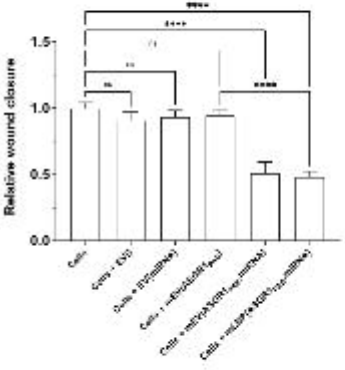
Relative wound closure
1.5
1.0
0.5
0.0

C

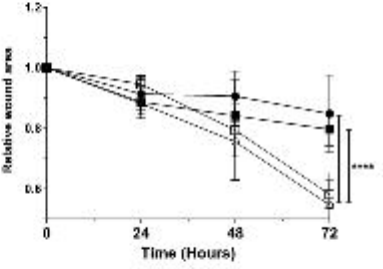
Relative wound area
1.2
1.0
0.8
0.6
0
24
48
72
Time (Hours)

Figure 6

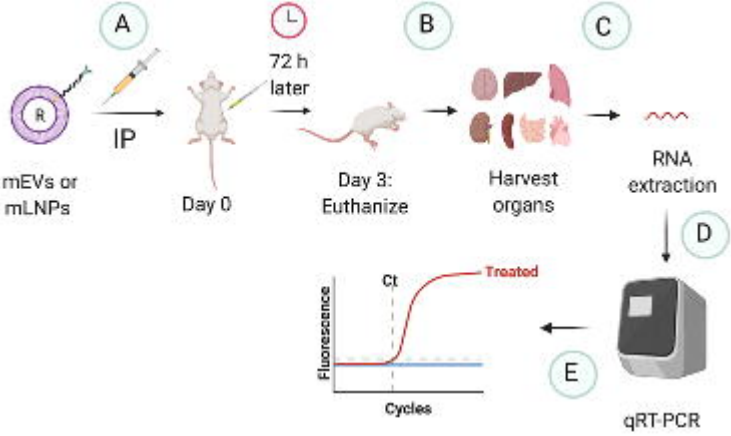
A
B
C
D
E
R
IP
mEVs or
mLNPs
Day 0
72 h
later
Day 3:
Euthanize
Harvest
organs
RNA
extraction
qRT-PCR
Ct
Treated
Fluorescence
Cycles

Figure 7

A

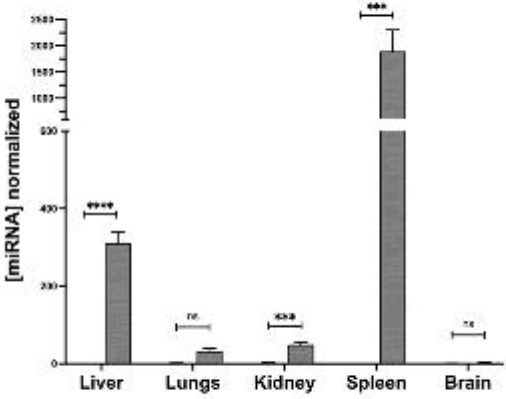
[miRNA] normalized
Liver
Lungs
Kidney
Spleen
Brain

B

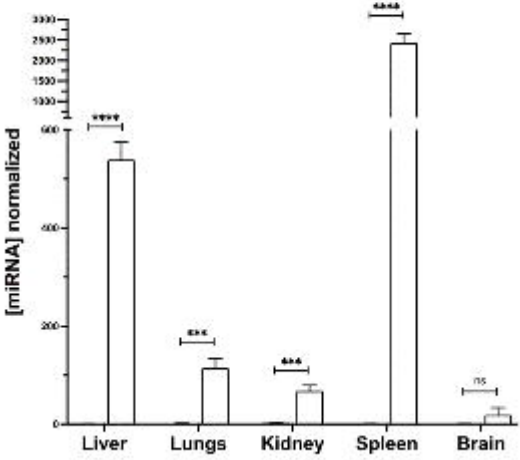
[miRNA] normalized
Liver
Lungs
Kidney
Spleen
Brain

Figure 8

A

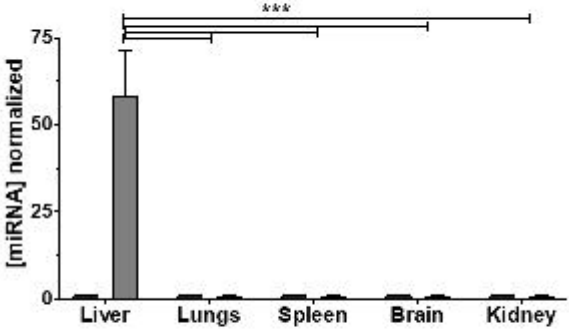
***
75
50
25
0
[miRNA] normalized
Liver
Lungs
Spleen
Brain
Kidney

B

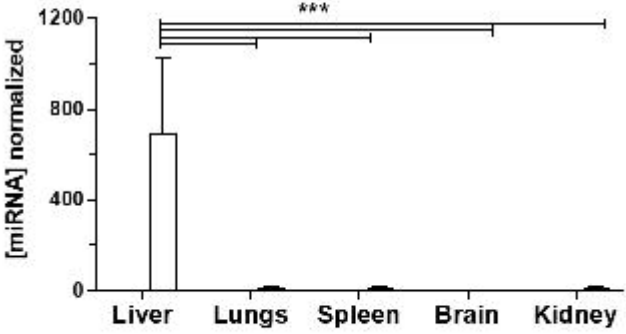
***
1200
800
400
0
[miRNA] normalized
Liver
Lungs
Spleen
Brain
Kidney

Figure 9

A

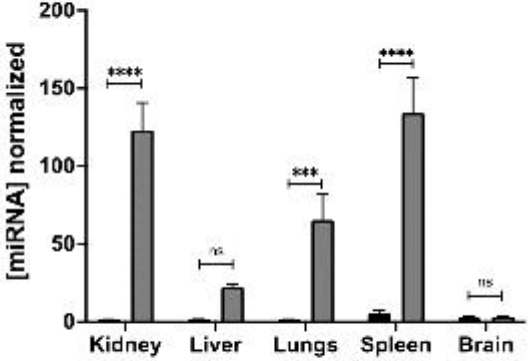
[miRNA] normalized
200
150
100
50
0
****
ns
***
****
ns
Kidney
Liver
Lungs
Spleen
Brain

B

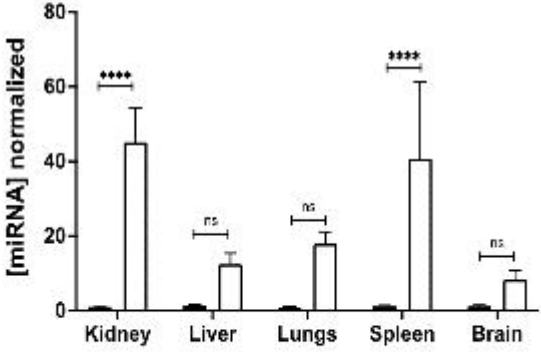
[miRNA] normalized
80
60
40
20
0
****
ns
ns
****
ns
Kidney
Liver
Lungs
Spleen
Brain

Figure 10

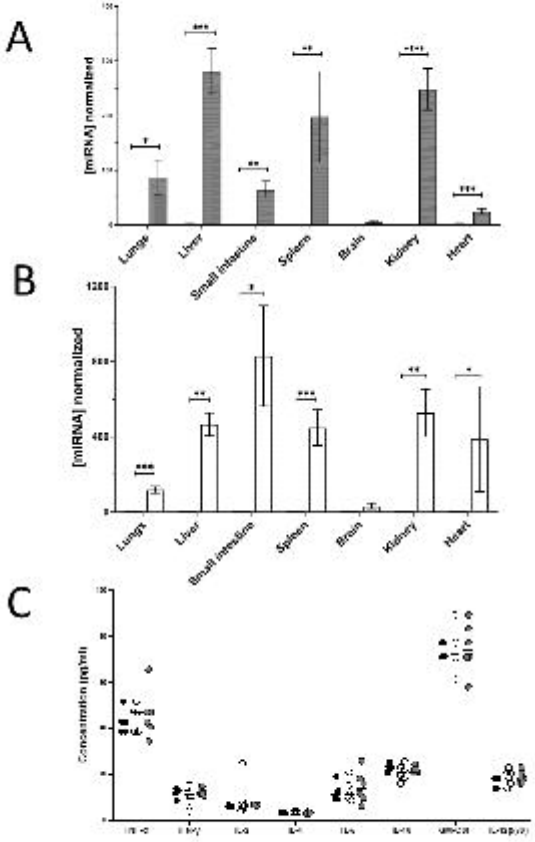
A
[mRNA] normalized
Lungs
Liver
Small intestine
Spleen
Brain
Kidney
Heart
B
[miRNA] normalized
Lungs
Liver
Small intestine
Spleen
Brain
Kidney
Heart
C
Concentration (ng/ml)